PHYSICAL REVIEW D **88,** 015017 (2013)

Single neutralino production at the LHC

A. I. Ahmadov[1,2,*] and M. Demirci[1,†]

[1]*Department of Physics, Karadeniz Technical University, 61080 Trabzon, Turkey*

[2]*Institute for Physical Problems, Baku State University, Z. Khalilov Street 23, AZ-1148 Baku, Azerbaijan*

(Received 14 January 2013; published 12 July 2013)

We consider that the direct production of a single neutralino in a proton-proton collision at the CERN Large Hadron Collider focusing on the lightest neutralino is possibly a candidate for dark matter and escapes detection. We present a comprehensive investigation of the dependence of total cross sections of the processes $pp(q\bar{q}) \to \tilde{\chi}_i^0 \tilde{g}$, $pp(qg) \to \tilde{\chi}_i^0 \tilde{q}_{L,R}$, and $pp(q\bar{q}') \to \tilde{\chi}_i^0 \tilde{\chi}_j^+$ at tree level and $pp(gg) \to \tilde{\chi}_i^0 \tilde{g}$ at one-loop level, on the center-of-mass energy, on the M_2-μ mass plane, on the squark mass, and on the $\tan\beta$ for the Constrained Minimal Supersymmetric Standard Model and three extremely different scenarios in the Minimal Supersymmetric Standard Model. In particular, the cross section of the process $pp \to \tilde{\chi}_2^0 \tilde{\chi}_1^+$ in the gauginolike scenario can reach about 0.6 (1.7) pb at a center-of-mass energy of $\sqrt{s} = 7(14)$ TeV. We extract therefrom that our results might lead to new aspects corresponding to experimental explorations, and these dependencies might be used as the bases of experimental research of the single neutralino production at hadron colliders.

DOI: 10.1103/PhysRevD.88.015017 PACS numbers: 11.30.Pb, 12.60.Jv, 14.80.Ly, 14.80.Nb

I. INTRODUCTION

The supersymmetric (SUSY) theories [1] have long been one of the leading candidates for new physics beyond the Standard Model (SM). They postulate the existence of SUSY particles (sparticles) whose spin differ by one-half unit with respect to that of their SM partner [2–4], and introducing these new particles provides solutions to the hierarchy problem. The existence of these supersymmetric particles can be determined at the Large Hadron Collider (LHC) and the International Linear Collider, who might supply the experimental facilities. However, even if most of the supersymmetric particles are produced at colliders, they will not be detected because they will eventually decay into the lightest supersymmetric particle (LSP) on the condition that the R parity [5,6] is conserved. As consequences of the R-parity conservation, sparticles can only be created (or destroyed) in pairs and the LSP is absolutely stable, which is generally assumed to be a weakly interacting massive particle, and so making it an excellent candidate for astrophysical dark matter [7,8] that is one of the attractive features of SUSY. In the majority of SUSY breaking models, the LSP is the lightest neutralino, and it occurs at the end of the decay chain of each supersymmetric particle. For these purposes, a detailed study of the lightest neutralino is of great importance for the theoretical and phenomenological aspects of SUSY.

Among all the supersymmetric models, the Minimal Supersymmetric Standard Model (MSSM), which is almost the direct version of the supersymmetric SM, has an extra Higgs doublet and general SUSY breaking soft terms. The superpartners of the Higgs doublets (Higgsinos) mix with the superpartners of the gauge bosons (gauginos) to form four Majorana mass eigenstates called neutralino $\tilde{\chi}_i^0$, $i = 1, 2, 3, 4$ and two charged mass eigenstates called charginos $\tilde{\chi}_j^{\pm}$, $j = 1, 2$ in the MSSM. The gaugino-Higgsino decomposition of the neutralinos and charginos includes significant knowledge regarding the mechanism of the supersymmetry breaking and plays an essential role in establishing the relic density of the dark matter [9].

The experimental explorations of the supersymmetric particles are among the main tasks of the experimental program at hadron colliders, especially at the LHC. Up to now, the ATLAS and CMS collaborations have chiefly concentrated on seeking the production of the strongly interacting squarks and gluinos. As a result, bounds on the masses of the squarks and gluinos are pushed to higher scales [10,11], and the experimental attention starts to go towards the production of the electroweak slepton, neutralino, and chargino.

The lower limit on the lightest neutralino mass ($m_{\tilde{\chi}_1^0}$) is given about 46 GeV at 95% confidence level, which can be obtained from the experimental bound on chargino mass in the MSSM at the large electron positron [12]. However, this limit increases to well above 100 GeV from the strong restrictions set by the recent LHC data in the framework of the constrained MSSM (CMSSM) containing both gaugino and sfermion mass unification [13].

In this paper, taking into account the allowed parameter space of the MSSM, we present numerical results for the single neutralino production processes in proton-proton collision at the LHC including a neutralino in the final state as follows: the associated subprocesses $q\bar{q} \to \tilde{\chi}_i^0 \tilde{g}$, $qg \to \tilde{\chi}_i^0 \tilde{q}_{L,R}$, $q\bar{q}' \to \tilde{\chi}_i^0 \tilde{\chi}_j^+$ at tree level and $gg \to \tilde{\chi}_i^0 \tilde{g}$ at one-loop level. There have been many works devoted to the study of these processes in the literature. For example,

*ahmadovazar@yahoo.com
†phy_mdemirci@yahoo.com

Refs. [14,15] focus on gluon/squark produced in association with charginos and neutralinos at proton-proton collision; Ref. [16] discusses the feasibility of SUSY monojet production at the LHC for measuring the neutralino-squark-quark coupling; the automized next-to-leading-order QCD and SUSY-QCD corrections to the squark-neutralino production are the focus of Ref. [17]; Refs. [18,19] search for associated production of charginos and neutralinos, and Ref. [20] focuses on single neutralino production.

One of the important approaches of our scenario consists of the mechanism of choosing the input parameters. Unlike the above works, in our study we have recovered the SUSY Lagrangian parameters as direct analytical expressions of suitable physical masses without constraining any of them in the MSSM so that we have principally concentrated on the algebraically nontrivial inversion for the gaugino mass parameters. In other words, using two chargino masses and $\tan\beta$ as input parameters, the other parameters we obtain are gaugino/Higgsino mass parameters, and the masses and mixing matrix of neutralino are outputs.

The neutralino mass eigenstates $\tilde{\chi}_i^0$ $(i = 1, \ldots, 4)$ are the linear superposition of the gauginos $\tilde{B}$, $\tilde{W}^3$ and the Higgsinos $\tilde{H}_1^0$, $\tilde{H}_2^0$ in the MSSM. In our case, the relative importance of the production mechanisms ($\tilde{q}_{L,R}$ and W^+) depends on the strengths of the $\tilde{B}$, $\tilde{W}^3$ and the Higgsinos $\tilde{H}_1^0$, $\tilde{H}_2^0$ components of the $\tilde{\chi}_i^0$; thus, significant differences in the cross sections are to be expected for the case of a gauginolike, Higgsino-like, and mixing neutralino, respectively. As we know, a supersymmetric neutralino is the standard candidate for weakly interacting massive particles dark matter. Despite this, it is still an open problem in SUSY.

By taking this information into account, it may be argued that the calculation and analysis of the single neutralino production at proton-proton collisions within the chosen scenarios is significant from both theoretical and experimental points of view. Accordingly, we investigate the dependence of total cross sections of the single neutralino production processes on the center-of-mass energy, the M_2-μ mass plane, the squark mass, and the $\tan\beta$ for CMSSM, and the three extremely different scenarios in the MSSM.

The layout of the paper is as follows: In Sec. II, we provide analytical expressions of the amplitudes and the cross sections of the relevant subprocesses and also the corresponding couplings. In Sec. III, we present detailed numerical results of the cross sections for each scenario and discuss the dependence of the cross section on the MSSM model parameters. Our conclusions are presented in Sec. IV. Finally, we summarize general information about the neutralino/chargino sector in the MSSM and present formulas related to obtaining neutralino masses in the Appendix.

II. ANALYTIC RESULTS OF THE CROSS SECTIONS FOR THE SINGLE NEUTRALINO PRODUCTION

In this section, we present succinct definitions of generalized corresponding to couplings in SUSY, and analytically expressions of the relating partonic cross sections for single neutralino production. Supplemental information about neutralinos at proton-proton collisions can be acquired from the single neutralino production triggered by the following subprocesses:

$$a^k(p_1)b^l(p_2) \to \begin{cases} \tilde{\chi}_i^0(k_1, E_1, m_i) & \tilde{\mathrm{g}}^m(k_2, E_2, m_j) \\ \tilde{\chi}_i^0(k_1, E_1, m_i) & \tilde{q}_{L,R}^m(k_2, E_2, m_j) \\ \tilde{\chi}_i^0(k_1, E_1, m_i) & \tilde{\chi}_j^{\pm}(k_2, E_2, m_j). \end{cases} \quad (2.1)$$

These are presented for the initial partons a, $b = q, \bar{q}$, g whose masses can be neglected. Here, p_1 and p_2 denote the four-momentum of the initial partons, and k_1 and k_2 represent the four-momentum of the two final states of a neutralino together with a gluino (or squark or chargino), respectively. We represent by k, l, m the color indices for the corresponding particles.

The Mandelstam variables for subprocesses (2.1) are given as

$$\hat{s} = (p_1 + p_2)^2, \qquad \hat{t} = (p_1 - k_1)^2, \qquad \hat{u} = (p_1 - k_2)^2. \quad (2.2)$$

Denoting by (p, θ) the momentum and scattering angle in the center-of-mass frame of the final states, we get center-of-mass energy and momentums as follows:

$$p = \frac{1}{2\sqrt{\hat{s}}}\sqrt{(\hat{s} - m_i^2 - m_j^2)^2 - 4m_i^2 m_j^2}, \quad E_1 = \frac{\hat{s} + m_i^2 - m_j^2}{2\sqrt{\hat{s}}},$$
$$E_2 = \frac{\hat{s} + m_j^2 - m_i^2}{2\sqrt{\hat{s}}}, \quad p_1 = \frac{\sqrt{\hat{s}}}{2}(1, 0, 0, 1),$$
$$p_2 = \frac{\sqrt{\hat{s}}}{2}(1, 0, 0, -1), \quad k_1 = (E_1, p\sin\theta, 0, p\cos\theta),$$
$$k_2 = (E_2, -p\sin\theta, 0, -p\cos\theta). \quad (2.3)$$

We give generalized electroweak couplings for the corresponding single neutralino production in the MSSM. The square of the weak coupling constant $g^2 = e^2/\sin^2\theta_W$ is defined in terms of the electromagnetic fine structure constant $\alpha = e^2/4\pi$ and electroweak mixing angle $c_W = \cos\theta_W$, $s_W = \sin\theta_W$. Following the standard notation, the W-chargino-neutralino interaction vertices are proportional to couplings as follows [3]:

$$O_{ij}^L = -\frac{c_W}{\sqrt{2}}N_{i4}V_{j2}^* + c_W N_{i2}V_{j1}^*,$$
$$O_{ij}^R = \frac{c_W}{\sqrt{2}}N_{i3}^* U_{j2} + c_W N_{i2}^* U_{j1}. \quad (2.4)$$

We neglect masses of the initial partons and generational mixing in the (s)quark sectors; the gaugino-squark-quark interaction vertices are proportional to the corresponding neutralino-squark-quark couplings [21,22],

$$\begin{aligned} C^L_{\tilde{\chi}^0_i \tilde{q} q} &= [(e_q - I^3_q) s_W N_{i1} + I^3_q c_W N_{i2}], \\ C^R_{\tilde{\chi}^0_i \tilde{q} q} &= -e_q s_W N^*_{i1}, \end{aligned} \tag{2.5}$$

and the corresponding chargino-squark-quark couplings (for q, $q' = u$, d quarks)

$$\begin{aligned} C^L_{\tilde{\chi}^+_j \tilde{q} q'} &= \frac{c_W}{\sqrt{2}}(U_{j1}\delta_{q'u} + V^*_{j1}\delta_{q'd}) \\ &\quad - \frac{c_W(m_d U_{j2}\delta_{q'u} + m_u V^*_{j2}\delta_{q'd})}{2m_W(\cos\beta\delta_{q'u} + \sin\beta\delta_{q'd})}, \\ C^R_{\tilde{\chi}^+_j \tilde{q} q'} &= -\frac{m_{q'} c_W(V^*_{j2}\delta_{q'u} + U_{j2}\delta_{q'd})}{2m_W(\sin\beta\delta_{q'u} + \cos\beta\delta_{q'd})}, \end{aligned} \tag{2.6}$$

where I^3_q is the weak isospin quantum number such that $I^3_q = \pm 1/2$ for left-handed and $I^3_q = 0$ for right-handed up- and down-type quarks, e_q denotes their fractional electromagnetic charge, and the matrices N, U and V are neutralino and chargino mixing matrices, respectively. The couplings of the neutralino to quark, squark, chargino, and W boson are determined by the corresponding elements of the mixing matrices (N_{ij},U_{ij}, V_{ij}), as shown in the above relations. The relevant couplings of the particles for single neutralino production are derived from the following interaction Lagrangians of the MSSM [3]:

$$\begin{aligned} L_{\tilde{\chi}^0_i \tilde{q} q} &= -\frac{\sqrt{2}g}{c_W}\bar{q}[C^{L*}_{\tilde{\chi}^0_i \tilde{q} q} P_L + C^{R*}_{\tilde{\chi}^0_i \tilde{q} q} P_R]\tilde{\chi}^0_i \tilde{q}_{L,R}, \\ L_{q\tilde{q}\,\tilde{\mathrm{g}}} &= -\sqrt{2}g_s T^a_{jk}[\bar{\tilde{\mathrm{g}}}_a P_L q^k \tilde{q}^{j*}_L + \bar{q}^j P_R \tilde{\mathrm{g}}_a \tilde{q}^k_L \\ &\quad - \bar{\tilde{\mathrm{g}}}_a P_R q^k \tilde{q}^{j*}_R - \bar{q}^j P_L \tilde{\mathrm{g}}_a \tilde{q}^k_R], \\ L_{\tilde{q}\,\tilde{q}\,\mathrm{g}} &= -ig_s G^a_\mu[\tilde{q}^{j*} T^a_{jk} \partial^\mu \tilde{q}^k - \partial^\mu \tilde{q}^{j*} T^a_{jk} \tilde{q}^k], \\ L_{W^+ \tilde{\chi}^0_i \tilde{\chi}^+_j} &= \frac{g}{c_W} W_\mu \overline{\tilde{\chi}^0_i} \gamma^\mu [O^L_{ij} P_L + O^R_{ij} P_R]\tilde{\chi}^+_j, \\ L_{\tilde{\chi}^+_j \tilde{q} q'} &= -\frac{\sqrt{2}g}{c_W}\bar{q}[C^{L*}_{\tilde{\chi}^+_j \tilde{q} q'} P_L + C^{R*}_{\tilde{\chi}^+_j \tilde{q} q'} P_R]\tilde{\chi}^+_j \tilde{q}_{L,R}, \end{aligned} \tag{2.7}$$

where $\tilde{\chi}^0_i$, $\tilde{\chi}^+_j$, q, $\tilde{q}_{L,R}$, and $\tilde{\mathrm{g}}$ are four-component spinor fields, $P_{R,L} = \frac{1}{2}(1 \pm \gamma^5)$, T^a_{jk} is a color generator, and strong coupling $g_s = \sqrt{4\pi\alpha_s}$. The running strong coupling constant α_s is given as follows:

$$\alpha_s(Q^2) = \frac{4\pi}{(11 - \frac{2}{3}n_f)\ln(Q^2/\Lambda^2)}, \tag{2.8}$$

where Λ is the QCD scale parameter, and n_f is the number of active flavors at the energy scale Q that can be chosen as the average of the final particle masses.

The total cross sections for the subprocesses can be obtained by using the following formula [23]:

$$\hat{\sigma}(\hat{s}) = \int_{\hat{t}^-}^{\hat{t}^+} d\hat{t} \frac{d\hat{\sigma}}{d\hat{t}}, \tag{2.9}$$

where $\hat{t}^\pm = 1/2[(m_i^2 + m_j^2 - \hat{s}) \pm \sqrt{(\hat{s} - m_i^2 - m_j^2)^2 - 4m_i^2 m_j^2}]$. With the results from Eq. (2.9) for the relevant subprocess, the total unpolarized hadronic cross sections in proton-proton collisions at center-of-mass energy can be calculated by

$$\sigma(s) = \int_{(m_i+m_j)^2/s}^1 d\tau \frac{d\mathcal{L}^{\mathrm{pp}}_{ab}}{d\tau} \hat{\sigma}\,(\text{subprocess, at } \hat{s} = \tau s), \tag{2.10}$$

with the parton luminosity

$$\begin{aligned} \frac{d\mathcal{L}^{\mathrm{pp}}_{ab}}{d\tau} &= \int_\tau^1 \frac{dx_1}{x_1} \frac{1}{1 + \delta_{ab}} \Big[G_{a/h_1}(x_1, \mu_F) G_{b/h_2}\Big(\frac{\tau}{x_1}, \mu_F\Big) \\ &\quad + G_{b/h_1}(x_1, \mu_F) G_{a/h_2}\Big(\frac{\tau}{x_1}, \mu_F\Big)\Big], \end{aligned} \tag{2.11}$$

where G_{a/h_1} and G_{b/h_2} are universal parton densities of the partons a, b in the hadrons h_1, h_2, which depend on the longitudinal momentum fractions of the two partons x_1, x_2 ($\tau = x_1 x_2$) at the unphysical factorization scale μ_F. We fix the factorization scale to the average mass of the final-state particles, $\mu_F = (m_i + m_j)/2$.

Considering each subprocess separately, we now present analytic expressions of the amplitudes and the differential cross sections for the single neutralino production in the following subsections.

A. The subprocess $q\bar{q} \to \tilde{\chi}^0_i \tilde{\mathrm{g}}$

The production of neutralino-gluino originates from quark-antiquark initial states through the tree-level Feynman diagrams shown in Fig. 1 and can be expressed as

$$q^k(p_1)\bar{q}^l(p_2) \to \tilde{\chi}^0_i(k_1)\tilde{\mathrm{g}}^m(k_2), \tag{2.12}$$

where p_1, p_2, k_1, and k_2 denote the four-momentum of the quark, antiquark, and the two final-state neutralino and gluino, respectively. Here, the color indices of the quark, antiquark, and gluino are denoted by k, l, and m, respectively. The mass m_j now denotes the mass of the gluino in Eq. (2.3) where the kinematic is defined.

In this case, the production occurs by quark-antiquark scattering via t channel (a) and u channel (b) squark exchange in a semistrong reaction. The tree-level contributions to the amplitude result from the two channels are

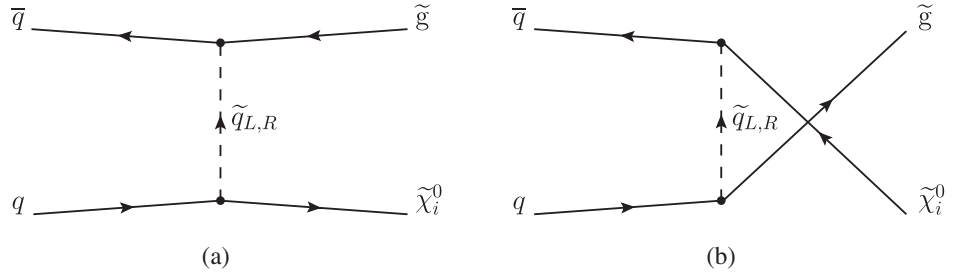

FIG. 1. Feynman diagrams of the subprocess $q\bar{q} \to \tilde{\chi}_i^0 \tilde{g}$ to leading level.

$$T_{\hat{t}} = \frac{2g_s g T^m_{lj}}{(\hat{t} - m^2_{\tilde{q}_L})c_W}[\bar{v}(p_2)P_R u^c_{\tilde{g}}(k_2)] \cdot [\bar{u}_{\tilde{\chi}_i^0}(k_1) C^L_{\tilde{\chi}_i^0 \tilde{q} q} P_L u(p_1)] - \frac{2g_s g T^m_{lj}}{(\hat{t} - m^2_{\tilde{q}_R})c_W}[\bar{v}(p_2)P_L u^c_{\tilde{g}}(k_2)] \cdot [\bar{u}_{\tilde{\chi}_i^0}(k_1) C^R_{\tilde{\chi}_i^0 \tilde{q} q} P_R u(p_1)], \quad (2.13)$$

$$T_{\hat{u}} = -\frac{2g_s g T^m_{kj}}{(\hat{u} - m^2_{\tilde{q}_L})c_W}[\bar{v}(p_2) C^{L*}_{\tilde{\chi}_i^0 \tilde{q} q} P_R u^c_{\tilde{\chi}_i^0}(k_1)] \cdot [\bar{u}_{\tilde{g}}(k_2) P_L u(p_1)] + \frac{2g_s g T^m_{kj}}{(\hat{u} - m^2_{\tilde{q}_R})c_W} \times [\bar{v}(p_2) C^{R*}_{\tilde{\chi}_i^0 \tilde{q} q} P_L u^c_{\tilde{\chi}_i^0}(k_1)] \cdot [\bar{u}_{\tilde{g}}(k_2) P_R u(p_1)], \quad (2.14)$$

where the superscript c denotes "charge conjugate spinor" defined by $\psi^c \equiv C\bar{\psi}^T$. In order to do the spin sums, we use the spinor completeness relations given as $u = C\bar{v}^T$ and $v = C\bar{u}^T$ for Majorana fermions [3]. The relevant couplings for this subprocess are given in Eq. (2.5). After averaging over spins and colors in the initial state, the analytic form of the partonic differential cross section for this subprocess is obtained from these amplitudes by using the following formula:

$$\frac{d\hat{\sigma}}{d\hat{t}}(q\bar{q} \to \tilde{\chi}_i^0 \tilde{g}) = \frac{1}{576\ \pi \hat{s}^2}(M_{\hat{t}\hat{t}} + M_{\hat{u}\hat{u}} - 2M_{\hat{t}\hat{u}}), \quad (2.15)$$

where

$$M_{\hat{t}\hat{t}} = \frac{16 g_s^2 g^2}{c_W^2}\left[\frac{|C^L_{\tilde{\chi}_i^0 \tilde{q} q}|^2}{(\hat{t} - m^2_{\tilde{q}_L})^2} + \frac{|C^R_{\tilde{\chi}_i^0 \tilde{q} q}|^2}{(\hat{t} - m^2_{\tilde{q}_R})^2}\right](m^2_{\tilde{\chi}_i^0} - \hat{t})(m^2_{\tilde{g}} - \hat{t}), \quad (2.16)$$

$$M_{\hat{u}\hat{u}} = \frac{16 g_s^2 g^2}{c_W^2}\left[\frac{|C^L_{\tilde{\chi}_i^0 \tilde{q} q}|^2}{(\hat{u} - m^2_{\tilde{q}_L})^2} + \frac{|C^R_{\tilde{\chi}_i^0 \tilde{q} q}|^2}{(\hat{u} - m^2_{\tilde{q}_R})^2}\right] \times (m^2_{\tilde{\chi}_i^0} - \hat{u})(m^2_{\tilde{g}} - \hat{u}), \quad (2.17)$$

$$M_{\hat{t}\hat{u}} = \frac{16 g_s^2 g^2}{c_W^2}\left[\frac{C^L_{\tilde{\chi}_i^0 \tilde{q} q} C^L_{\tilde{\chi}_i^0 \tilde{q} q}}{(\hat{t} - m^2_{\tilde{q}_L})(\hat{u} - m^2_{\tilde{q}_L})} + \frac{C^R_{\tilde{\chi}_i^0 \tilde{q} q} C^R_{\tilde{\chi}_i^0 \tilde{q} q}}{(\hat{t} - m^2_{\tilde{q}_R})(\hat{u} - m^2_{\tilde{q}_R})}\right] \times (m_{\tilde{\chi}_i^0} m_{\tilde{g}} \hat{s}). \quad (2.18)$$

B. The subprocess $qg \to \tilde{\chi}_i^0 \tilde{q}_{L,R}$

The associated production of neutralino and squark, which can be produced via quark-gluon scattering, can be expressed through the following subprocess:

$$q^k(p_1) g^l(p_2) \to \tilde{\chi}_i^0(k_1) \tilde{q}^m_{L,R}(k_2), \quad (2.19)$$

where p_1 and p_2 denote the four-momentum of the two initial-state quark and gluon, and k_1 and k_2 denote the four-momentum of neutralino and squark in the final state, respectively. We denote by k, l, and m as the color indices of the quark, gluon, and squark, respectively. In Eq. (2.3), the mass m_j now describes the squark mass.

The tree-level Feynman diagrams of the subprocess are displayed in Fig. 2. This subprocess receives s-channel contribution from the exchange of quark, as well as

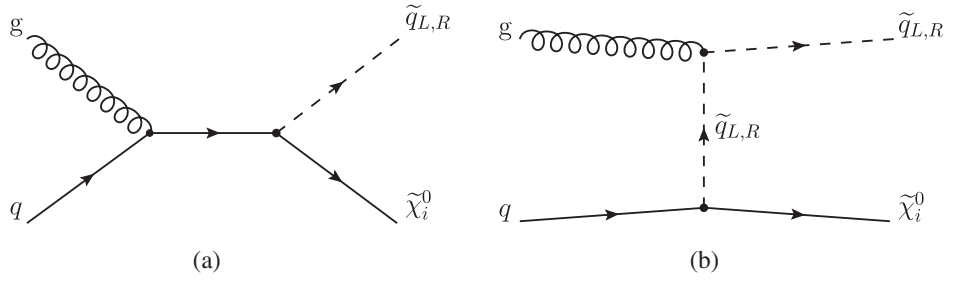

FIG. 2. Feynman diagrams of the subprocess $qg \to \tilde{\chi}_i^0 \tilde{q}_{L,R}$ to leading level.

t-channel contribution via exchange of the left- and right-handed squark $\tilde{q}_{L,R}$. The leading-level contributions to the amplitude arising from the two diagrams in Fig. 2 are

$$T_{\hat{s}} = -\frac{\sqrt{2}g_s g T^l_{kj}}{\hat{s}c_W}[\bar{u}_{\tilde{\chi}^0_i}(k_1)(C^L_{\tilde{\chi}^0_i\tilde{q}q}P_L + C^R_{\tilde{\chi}^0_i\tilde{q}q}P_R) \times (\not{p}_1 + \not{p}_2)\not{\epsilon}_2 u(p_1)], \tag{2.20}$$

$$T_{\hat{t}} = -\frac{\sqrt{2}g_s g T^l_{mj}}{c_W}\left[\bar{u}_{\tilde{\chi}^0_i}(k_1)\left\{\frac{C^L_{\tilde{\chi}^0_i\tilde{q}q}P_L}{(\hat{t}-m^2_{\tilde{q}_L})} + \frac{C^R_{\tilde{\chi}^0_i\tilde{q}q}P_R}{(\hat{t}-m^2_{\tilde{q}_R})}\right\}u(p_1)\right] \times (2\epsilon_2\cdot k_2), \tag{2.21}$$

where ϵ_2 denotes the polarization vector of the initial gluon. The relevant couplings are given in Eq. (2.5). After averaging over spins and colors in the initial state, the parton-level differential cross section for this subprocess takes the form

$$\frac{d\hat{\sigma}}{d\hat{t}}(qg \to \tilde{\chi}^0_i\tilde{q}_{L,R}) = \frac{1}{1536\ \pi\hat{s}^2}(M_{\hat{s}\hat{s}} + M_{\hat{t}\hat{t}} + 2M_{\hat{s}\hat{t}}), \tag{2.22}$$

where

$$M_{\hat{s}\hat{s}} = \frac{16g_s^2g^2}{\hat{s}^2c_W^2}[|C^L_{\tilde{\chi}^0_i\tilde{q}q}|^2 + |C^R_{\tilde{\chi}^0_i\tilde{q}q}|^2](m^2_{\tilde{\chi}^0_i} - \hat{u})\hat{s}, \tag{2.23}$$

$$M_{\hat{t}\hat{t}} = \frac{32g_s^2g^2}{c_W^2}\left[\frac{|C^L_{\tilde{\chi}^0_i\tilde{q}q}|^2m^2_{\tilde{q}_L}}{(\hat{t}-m^2_{\tilde{q}_L})^2} + \frac{|C^R_{\tilde{\chi}^0_i\tilde{q}q}|^2m^2_{\tilde{q}_R}}{(\hat{t}-m^2_{\tilde{q}_R})^2}\right](\hat{t} - m^2_{\tilde{\chi}^0_i}), \tag{2.24}$$

$$M_{\hat{s}\hat{t}} = \frac{8g_s^2g^2}{c_W^2}\left[\frac{|C^L_{\tilde{\chi}^0_i\tilde{q}q}|^2}{(\hat{t}-m^2_{\tilde{q}_L})\hat{s}} + \frac{|C^R_{\tilde{\chi}^0_i\tilde{q}q}|^2}{(\hat{t}-m^2_{\tilde{q}_R})\hat{s}}\right] \times [(m^2_{\tilde{\chi}^0_i} - \hat{u})(m^2_{\tilde{\chi}^0_i} - \hat{t}) - \hat{s}(m^2_{\tilde{\chi}^0_i} - \hat{t}) - \hat{s}m^2_{\tilde{\chi}^0_i}]. \tag{2.25}$$

C. The subprocess $q\bar{q}' \to \tilde{\chi}^0_i\tilde{\chi}^+_j$

The neutralino and chargino production, which can dominantly be produced by annihilation of quarks and antiquarks at hadron colliders is as follows:

$$q(p_1)\bar{q}'(p_2) \to \tilde{\chi}^0_i(k_1)\tilde{\chi}^+_j(k_2), \tag{2.26}$$

where particle labels denote the corresponding four-momentum. The kinematic is defined in Eq. (2.3), with m_i denoting the neutralino mass and m_j the chargino mass. The neutralino-chargino production occurs via the Feynman diagrams shown in Fig. 3. This subprocess proceeds at tree level via the vector boson W^+ exchange in the s channel and via t- and u-channel exchange of the left squark $\tilde{u}_L$ and $\tilde{d}_L$. The tree-level contributions to the amplitude arising from the three diagrams in Fig. 3 are

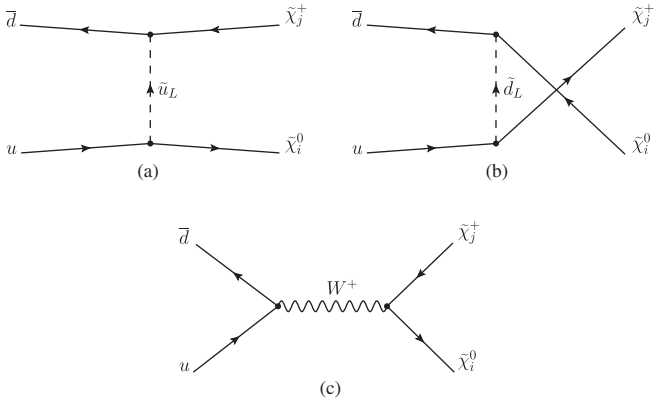

FIG. 3. Feynman diagrams of the subprocess $u\bar{d} \to \tilde{\chi}^0_i\tilde{\chi}^+_j$ to leading level.

$$T_{\hat{s}} = -\frac{g^2}{c_W^2}D_W(\hat{s})[\bar{u}_i(k_1)\gamma_\mu(O^L_{ij}P_L + O^R_{ij}P_R)v_j(k_2)] \cdot [\bar{v}(p_2)\gamma^\mu(L_{Wqq'}P_L + R_{Wqq'}P_R)u(p_1)], \tag{2.27}$$

$$T_{\hat{t}} = \frac{2g^2}{(\hat{t}-m^2_{\tilde{q}_L})c_W^2}[\bar{u}_i(k_1)(C^{L*}_{\tilde{\chi}^0_i\tilde{q}q}P_L + C^{R*}_{\tilde{\chi}^0_i\tilde{q}q}P_R)u(p_1)] \cdot [\bar{v}(p_2)\gamma^\mu(C^L_{\tilde{\chi}^+_j\tilde{q}q'}P_L + C^R_{\tilde{\chi}^+_j\tilde{q}q'}P_R)v_j(k_2)], \tag{2.28}$$

$$T_{\hat{u}} = \frac{2g^2}{(\hat{u}-m^2_{\tilde{q}'_L})c_W^2}[\bar{u}_j(k_2)(C^{L*}_{\tilde{\chi}^+_j\tilde{q}'q}P_L + C^{R*}_{\tilde{\chi}^+_j\tilde{q}'q}P_R)u(p_1)] \cdot [\bar{v}(p_2)\gamma^\mu(C^L_{\tilde{\chi}^0_i\tilde{q}'q'}P_L + C^R_{\tilde{\chi}^0_i\tilde{q}'q'}P_R)v_i(k_1)]. \tag{2.29}$$

In order to obtain the cross section for this subprocess, one would have to calculate the couplings of the neutralino-quark-squark, chargino-quark-squark, and neutralino-chargino-W^+ boson. We summarize these couplings in Eqs. (2.4)–(2.6). The analytic form of the partonic differential cross section after spin and color averaging reads

$$\frac{d\hat{\sigma}}{d\hat{t}}(q\bar{q}' \to \tilde{\chi}^0_i\tilde{\chi}^+_j) = \frac{1}{192\ \pi\hat{s}^2}(M_{\hat{s}\hat{s}} + M_{\hat{t}\hat{t}} + M_{\hat{u}\hat{u}} - 2M_{\hat{s}\hat{t}} + 2M_{\hat{s}\hat{u}} - 2M_{\hat{t}\hat{u}}), \tag{2.30}$$

where

$$\begin{aligned} M_{\hat{s}\hat{s}} = \frac{4g^2|D_W(\hat{s})|^2}{c_W^4}\{&[L^2_{Wqq'} + R^2_{Wqq'}] \\ &\times [O^L_{ij}O^{R*}_{ij} + O^{L*}_{ij}O^R_{ij}]m_{\tilde{\chi}^0_i}m_{\tilde{\chi}^+_j}\hat{s} \\ &+ [|O^L_{ij}|^2L^2_{Wqq'} + |O^R_{ij}|^2R^2_{Wqq'}](m^2_{\tilde{\chi}^0_i} - \hat{u})(m^2_{\tilde{\chi}^+_j} - \hat{u}) \\ &+ [|O^L_{ij}|^2R^2_{Wqq'} + |O^R_{ij}|^2L^2_{Wqq'}](m^2_{\tilde{\chi}^0_i} - \hat{t})(m^2_{\tilde{\chi}^+_j} - \hat{t})\}, \end{aligned} \tag{2.31}$$

$$M_{\hat{t}\hat{t}} = \frac{4g^2}{(\hat{t}-m^2_{\tilde{q}_L})^2 c_W^4}[|C^L_{\tilde{\chi}^0_i \tilde{q} q}|^2 + |C^R_{\tilde{\chi}^0_i \tilde{q} q}|^2][|C^L_{\tilde{\chi}^+_j \tilde{q} q'}|^2 + |C^R_{\tilde{\chi}^+_j \tilde{q} q'}|^2](m^2_{\tilde{\chi}^0_i}-\hat{t})(m^2_{\tilde{\chi}^+_j}-\hat{t}), \quad (2.32)$$

$$M_{\hat{u}\hat{u}} = \frac{4g^2}{(\hat{u}-m^2_{\tilde{q}'_L})^2 c_W^4}[|C^L_{\tilde{\chi}^+_j \tilde{q}' q}|^2 + |C^R_{\tilde{\chi}^+_j \tilde{q}' q}|^2][|C^L_{\tilde{\chi}^0_i \tilde{q}' q'}|^2 + |C^R_{\tilde{\chi}^0_i \tilde{q}' q'}|^2](m^2_{\tilde{\chi}^0_i}-\hat{u})(m^2_{\tilde{\chi}^+_j}-\hat{u}), \quad (2.33)$$

$$\begin{aligned} M_{\hat{t}\hat{u}} = \frac{4g^2}{(\hat{t}-m^2_{\tilde{q}_L})(\hat{u}-m^2_{\tilde{q}'_L})c_W^4}\Big\{\frac{1}{2}\Big[&C^{L*}_{\tilde{\chi}^0_i \tilde{q} q} C^{L*}_{\tilde{\chi}^0_i \tilde{q}' q'} C^L_{\tilde{\chi}^+_j \tilde{q}' q} C^L_{\tilde{\chi}^+_j \tilde{q} q'} \\ &+ C^{R*}_{\tilde{\chi}^0_i \tilde{q} q} C^{R*}_{\tilde{\chi}^0_i \tilde{q}' q'} C^R_{\tilde{\chi}^+_j \tilde{q}' q} C^R_{\tilde{\chi}^+_j \tilde{q} q'}\Big]\Big[\Big(m^2_{\tilde{\chi}^0_i}-\hat{u}\Big)\Big(m^2_{\tilde{\chi}^+_j}-\hat{u}\Big) \\ &+ \Big(m^2_{\tilde{\chi}^0_i}-\hat{t}\Big)\Big(m^2_{\tilde{\chi}^+_j}-\hat{t}\Big) - \hat{s}\Big(\hat{s}-m^2_{\tilde{\chi}^0_i}-m^2_{\tilde{\chi}^+_j}\Big)\Big] \\ &+ m_{\tilde{\chi}^0_i} m_{\tilde{\chi}^+_j}\hat{s}\Big[C^{L*}_{\tilde{\chi}^0_i \tilde{q} q} C^{R*}_{\tilde{\chi}^0_i \tilde{q}' q'} C^L_{\tilde{\chi}^+_j \tilde{q}' q} C^R_{\tilde{\chi}^+_j \tilde{q} q'} \\ &+ C^{R*}_{\tilde{\chi}^0_i \tilde{q} q} C^{L*}_{\tilde{\chi}^0_i \tilde{q}' q'} C^R_{\tilde{\chi}^+_j \tilde{q}' q} C^L_{\tilde{\chi}^+_j \tilde{q} q'}\Big]\Big\}, \end{aligned} \quad (2.34)$$

$$\begin{aligned} M_{\hat{s}\hat{u}} = \frac{-4g^4(\mathrm{Re}[D_W(\hat{s})])}{(\hat{u}-m^2_{\tilde{q}'_L})c_W^4}\Big\{\Big[&L_{W q q'} O^R_{ij} C^{L*}_{\tilde{\chi}^0_i \tilde{q}' q'} C^L_{\tilde{\chi}^+_j \tilde{q}' q} \\ &+ R_{W q q'} O^L_{ij} C^{R*}_{\tilde{\chi}^0_i \tilde{q}' q'} C^R_{\tilde{\chi}^+_j \tilde{q}' q}\Big]\Big(m^2_{\tilde{\chi}^0_i}-\hat{u}\Big)\Big(m^2_{\tilde{\chi}^+_j}-\hat{u}\Big) \\ &+ m_{\tilde{\chi}^0_i} m_{\tilde{\chi}^+_j}\hat{s}\Big[L_{W q q'} O^L_{ij} C^{L*}_{\tilde{\chi}^0_i \tilde{q}' q'} C^L_{\tilde{\chi}^+_j \tilde{q}' q} \\ &+ R_{W q q'} O^R_{ij} C^{R*}_{\tilde{\chi}^0_i \tilde{q}' q'} C^R_{\tilde{\chi}^+_j \tilde{q}' q}\Big]\Big\}, \end{aligned} \quad (2.35)$$

$$\begin{aligned} M_{\hat{s}\hat{t}} = \frac{-4g^4(\mathrm{Re}[D_W(\hat{s})])}{(\hat{t}-m^2_{\tilde{q}_L})c_W^4}\Big\{\Big[&L_{W q q'} O^R_{ij} C^L_{\tilde{\chi}^0_i \tilde{q} q} C^{L*}_{\tilde{\chi}^+_j \tilde{q} q'} \\ &+ R_{W q q'} O^L_{ij} C^R_{\tilde{\chi}^0_i \tilde{q} q} C^{R*}_{\tilde{\chi}^+_j \tilde{q} q'}\Big]\Big(m^2_{\tilde{\chi}^0_i}-\hat{t}\Big)\Big(m^2_{\tilde{\chi}^+_j}-\hat{t}\Big) \\ &+ m_{\tilde{\chi}^0_i} m_{\tilde{\chi}^+_j}\hat{s}\Big[L_{W q q'} O^L_{ij} C^L_{\tilde{\chi}^0_i \tilde{q} q} C^{L*}_{\tilde{\chi}^+_j \tilde{q} q'} \\ &+ R_{W q q'} O^R_{ij} C^R_{\tilde{\chi}^0_i \tilde{q} q} C^{R*}_{\tilde{\chi}^+_j \tilde{q} q'}\Big]\Big\}. \end{aligned} \quad (2.36)$$

In the above relations, the following abbreviation has been used $D_W(\hat{s}) = \frac{1}{\hat{s}-m^2_W+im_W\Gamma_W}$, which is the W-boson propagator denominator. We get $m_W = 80.385$ GeV and the width of this boson is $\Gamma_W = 2.085$ GeV for calculations.

D. The subprocess $gg \to \tilde{\chi}^0_i \tilde{g}$

The associated production of neutralino and gluino can be produced via the collision of gluon-gluon as follows:

$$g^k(p_1) g^l(p_2) \to \tilde{\chi}^0_i(k_1) \tilde{g}^m(k_2), \quad (2.37)$$

where p_1 and p_2 denote the four-momentum of the initial gluons, and k_1 and k_2 represent the four-momentum of the two final-state neutralino and gluino, respectively. We denote by k, l, and m the color indices of gluons and gluino, respectively. This subprocess first emerges at the one-loop level. We have performed the numerical evaluation for the subprocess $gg \to \tilde{\chi}^0_i \tilde{g}$ at one loop using the Mathematica packages FEYNARTS [24] to calculate corresponding amplitudes, FORMCALC [25,26] to produce a complete FORTRAN code containing the squared matrix elements, and LOOPTOOLS [27] to perform the evaluation of the necessary loop integrals. Also, the Feynman diagrams depicted in Fig. 4 have been generated by using FEYNARTS. In general, the one-loop corrections to subprocess $gg \to \tilde{\chi}^0_i \tilde{g}$ could be classified as vertex contributions and box contributions. The calculations of this subprocess have been carried out in the 't Hooft-Feynman gauge in which the gluon polarization sum is $\sum_\lambda \epsilon^*_\mu(k,\lambda)\epsilon_\nu(k,\lambda) = -g_{\mu\nu}$. For regularization of the ultraviolet divergences, we have used the constrained differential renormalization [28], which has been shown to be equivalent to regularization by dimensional reduction [29,30] at the one-loop level. Therefore, a supersymmetry-preserving regularization scheme is ensured via the implementation given in Ref. [31]. We do not display the analytical results of this process due to the fact that these are too long to be included here.

III. NUMERICAL ANALYSIS AND DISCUSSIONS

We now present numerical predictions for the cross sections of the single neutralino production in pp collisions at the LHC energies. We investigate the direct production of a single neutralino $\tilde{\chi}^0_i$ for first-generation quarks at hadron colliders focusing on the $\tilde{\chi}^0_1$ that is likely to be the LSP and $\tilde{\chi}^0_2$. The relevant subprocesses are $q\bar{q} \to \tilde{\chi}^0_i \tilde{g}$, $qg \to \tilde{\chi}^0_i \tilde{q}_{L,R}$, and $q\bar{q}' \to \tilde{\chi}^0_i \tilde{\chi}^\pm_j$ at tree level, while $gg \to \tilde{\chi}^0_i \tilde{g}$ at one-loop level, which could lead to the first detection of the supersymmetric particles at the LHC. In the numerical calculations, we just limit the values of the mass parameters M_1, M_2, and μ to be real, positive, and below 1 TeV, and get $\tan\beta = 45$, $m_{\tilde{u}_R} = 799.2$ GeV, $m_{\tilde{u}_L} = 798.2$ GeV, $m_{\tilde{d}_R} = 802.3$ GeV, $m_{\tilde{d}_L} = 800.3$ GeV, and $m_{\tilde{g}} = 1400$ GeV. For the other parameters, we use the values given by the Particle Data Group, such as $m_Z = 91.1876$ GeV, $m_W = 80.399$ GeV [13]. By using Eqs. (A13) and (A14) with two chargino masses, one could have three choices of parameter sets for the gaugino/Higgsino mass parameters M_2 and μ in three different cases, which are the gauginolike, the Higgsino-like, and the mixture case, respectively. We fix masses of the charginos as $m_{\tilde{\chi}^\pm_1} = 168.51$ GeV and $m_{\tilde{\chi}^\pm_2} = 295.01$ GeV for gaugino and Higgsino-like scenarios, and $m_{\tilde{\chi}^\pm_1} = 173.66$ GeV and $m_{\tilde{\chi}^\pm_2} = 289.86$ GeV for the mixture case. For each scenario, neutralino masses are calculated by inserting the values of M_2 and μ into Eq. (A8). Table I shows the gaugino/Higgsino and neutralino masses.

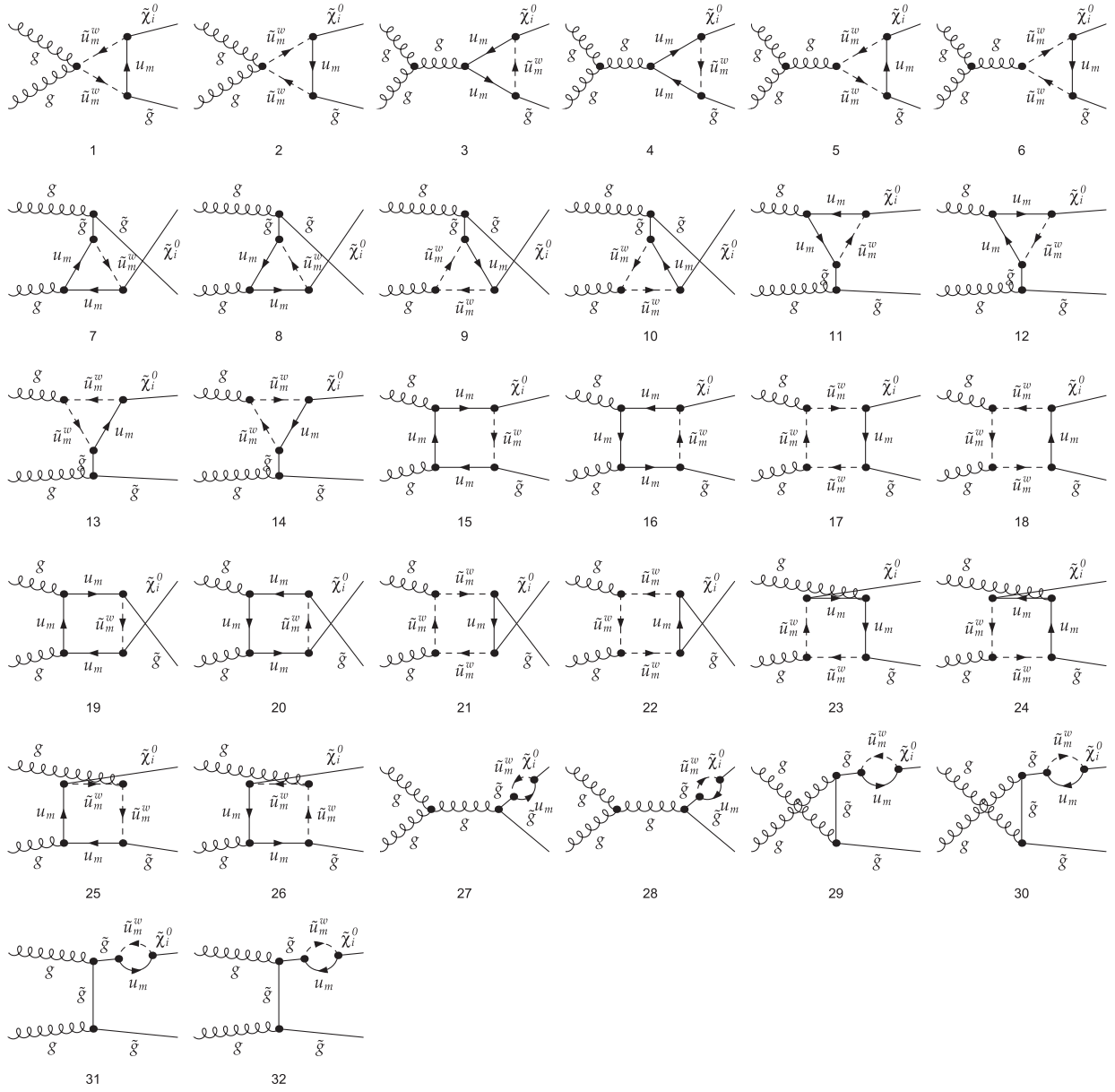

FIG. 4. Feynman diagrams of the subprocess $gg \to \tilde{\chi}_i^0 \tilde{g}$ to one-loop level. Also, this subprocess contains diagrams which are obtained by the replacements $u_m \to d_m$ and $\tilde{u}_m^w \to \tilde{d}_m^w$ in the above diagrams. Here, m and w indices denote the generation of (s)quark and the mass eigenstate of squark, respectively.

For comparison, we have also worked out the cross sections in the CMSSM 40.2.2 benchmark point [32] in the framework of the CMSSM [33–35] with five input parameters, namely, $m_0 = 600$ GeV, $m_{1/2} = 500$ GeV, $A_0 = -500$ GeV, $\tan\beta = 40$, and $\mu > 0$, where the parameters m_0 and $m_{1/2}$ are the universal scalar and gaugino mass parameters, A_0 is the universal trilinear soft SUSY breaking parameter, $\tan\beta$ is the ratio of the vacuum expectation values of the two Higgs doublets, and $\mathrm{sign}(\mu)$ is the sign of the Higgs mixing parameter. The universal parameters m_0, $m_{1/2}$, and A_0 are thought to appear by means of some gravity-mediated mechanism and are defined at the grand unified theories scale, whereas $\tan\beta$ and sign of the Higgs mixing parameter $\mathrm{sign}(\mu)$ are defined at the electroweak scale. All the masses and couplings of the model from these five parameters are obtained by the evolution from the grand unified theories scale down to the electroweak scale [36]. In this case, we have computed the SUSY particle spectrum by using the SOFTSUSY-3.3.4 package [37]. For the CMSSM 40.2.2 benchmark point, the gaugino masses M_2 and M_1, the Higgsino mass μ, and neutralino masses are given in Table I, and the other parameters are obtained as $m_{\tilde{\chi}_1^+} = 397.33$ GeV, $m_{\tilde{\chi}_2^+} = 711.85$ GeV, $m_{\tilde{u}_L} = 1199.95$ GeV, $m_{\tilde{d}_L} = 1202.41$ GeV,

TABLE I. The gaugino/Higgsino mass parameters and neutralino masses for each scenario.

(in GeV)	M_2	μ	M_1	$m_{\tilde{\chi}_1^0}$	$m_{\tilde{\chi}_2^0}$	$m_{\tilde{\chi}_3^0}$	$m_{\tilde{\chi}_4^0}$
Higgsino like	250.00	200.00	119.33	109.59	174.50	209.65	294.88
Gaugino like	200.00	250.00	95.46	91.50	169.50	259.40	293.85
Mixture case	225.00	225.00	107.39	101.42	176.13	234.52	289.37
CMSSM 40.2.2	391.24	698.59	210.84	208.23	397.26	702.97	711.31

$m_{\tilde{u}_R} = 1167.94$ GeV, $m_{\tilde{d}_R} = 1165.21$ GeV, and $m_{\tilde{g}} = 1170.38$ GeV.

We use the MSTW 2008 parton distribution functions [38] for the quark/gluon distributions inside the proton and fix the renormalization and factorization scales to the average final-state mass in our numerical calculations. For each scenario given above, we have numerically evaluated the hadronic cross sections of the single neutralino production processes involving a neutralino $\tilde{\chi}_1^0$ or $\tilde{\chi}_2^0$ in the final state, as a function of the center-of-mass energy from Figs. 5–8, the M_2-μ mass plane from Figs. 9–12, the squark mass from Figs. 13–16, and $\tan\beta$ from Figs. 17–20. In some of the figures, we use abbreviations as follows: Higgsino-like (HL) (solid line), gauginolike (GL) (dashed line), mixture-case (MC) (dotted-line), and CMSSM 40.2.2 benchmark point (CMSSM) (dot-dashed line), respectively. We now offer the following analysis of these figures in detail, separately.

In Figs. 5–8, we plot the dependence of the total cross sections for the single neutralino processes of the center-of-mass energy. These figures indicate that the total cross sections increase slowly and smoothly with increasing the beam energy from 7 to 14 TeV for each scenario. The CMSSM 40.2.2 benchmark point and gauginolike scenario are dominant for $pp \to \tilde{\chi}_i^0 \tilde{g}$ and $pp \to \tilde{\chi}_i^0 \tilde{q}_{L,R}$, respectively; however, in the associated production of a chargino with $\tilde{\chi}_i^0$, these dominancies vary such that the gauginolike scenario is dominant for $pp \to \tilde{\chi}_1^+ \tilde{\chi}_2^0$ and $\tilde{\chi}_2^+ \tilde{\chi}_1^0$, while the Higgsino-like and mixture-case scenarios are dominant for $pp \to \tilde{\chi}_1^+ \tilde{\chi}_1^0$ and $\tilde{\chi}_2^+ \tilde{\chi}_2^0$ because of contributions to the cross section from not only the neutralino mixing matrix but also from the chargino mixing matrixes. The difference of the cross sections in the scenarios comes only from the change of the couplings given in Eqs. (2.4)–(2.6) where the mixing matrices are changed. For cross sections of the process $gg \to \tilde{\chi}_i^0 \tilde{g}$ at one loop, the Higgsino-like scenario is larger than the other scenarios. As shown in Fig. 5, the cross section of the process $pp \to \tilde{\chi}_1^0 \tilde{g}$ in the CMSSM 40.2.2 benchmark point is about 9 times larger than in the gauginolike, Higgsino-like, and mixture-case scenarios. Also, the cross section of the process $pp \to \tilde{\chi}_2^0 \tilde{g}$ in the CMSSM 40.2.2 benchmark point is 7, 9, and 11 times larger than in the gauginolike, mixture-case, and Higgsino-like scenarios, respectively. As seen in Fig. 6, the cross section of the process $pp \to \tilde{\chi}_1^0 \tilde{q}_{L,R}$ in the gauginolike scenarios is about 17%, 6%, and 4 times larger than in the Higgsino-like scenario, mixture-case scenario, and CMSSM 40.2.2 benchmark point, respectively. Also, the cross section of the process $pp \to \tilde{\chi}_2^0 \tilde{q}_{L,R}$ in the gaugino-like scenario is 87%, 34%, and 5 times larger than in the Higgsino-like scenario, mixture-case scenarios, and CMSSM 40.2.2 benchmark point, respectively. It can be

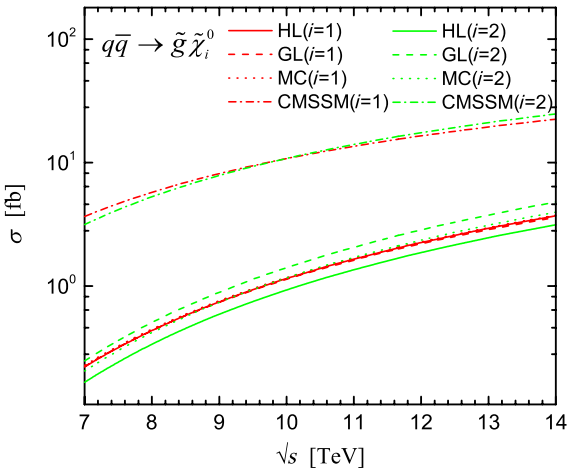

FIG. 5 (color online). Total cross sections of the process $pp \to \tilde{g}\tilde{\chi}_i^0$ ($i = 1, 2$) versus the center-of-mass energy of pp collider $\sqrt{s}$.

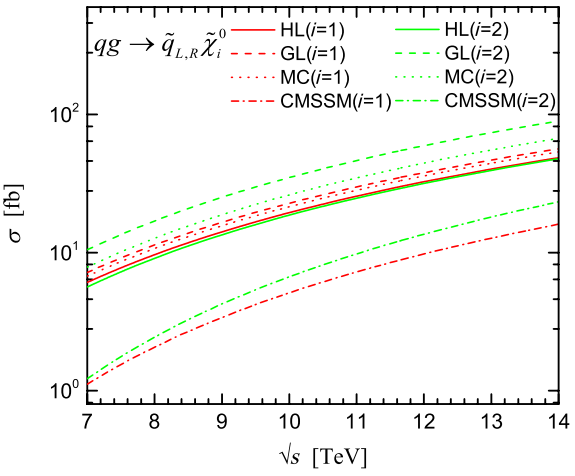

FIG. 6 (color online). Total cross sections for the process $pp \to \tilde{q}_{L,R}\tilde{\chi}_i^0$ ($i = 1, 2$) versus the center-of-mass energy of pp collider $\sqrt{s}$.

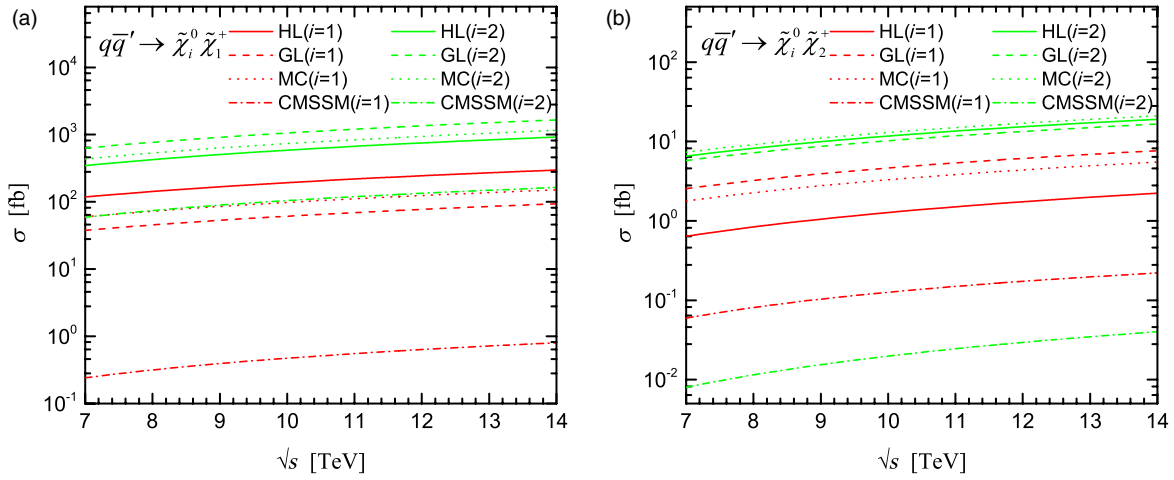

FIG. 7 (color online). Total cross sections of the processes $pp \to \tilde{\chi}_i^0 \tilde{\chi}_1^+$ (a) and $\tilde{\chi}_i^0 \tilde{\chi}_2^+$ (b) ($i = 1, 2$) versus the center-of-mass energy of pp collider $\sqrt{s}$.

seen from Fig. 7(a) that the cross section of the process $pp \to \tilde{\chi}_1^0 \tilde{\chi}_1^+$ in the Higgsino-like scenario is 3.2 times, 96%, and 3 orders of magnitude larger than in the gaugino-like scenario, mixture-case scenario, and CMSSM 40.2.2 benchmark point, respectively. The cross section of the process $pp \to \tilde{\chi}_2^0 \tilde{\chi}_1^+$ in the gauginolike scenario is roughly 2 times, 44%, and 1 order of magnitude larger than in the Higgsino-like scenario, mixture-case scenario, and CMSSM 40.2.2 benchmark point, respectively. Also, as shown in Fig. 7(b), the cross section of the process $pp \to \tilde{\chi}_1^0 \tilde{\chi}_2^+$ in the gauginolike scenario is roughly 3.6 times, 1.4 times, and 1 order of magnitude larger than in the Higgsino-like scenario, mixture-case scenario, and CMSSM 40.2.2 benchmark point, respectively. The cross section of the process $pp \to \tilde{\chi}_2^0 \tilde{\chi}_2^+$ in the mixture-case scenario is roughly 11%, 27%, and 3 orders of magnitude larger than in the Higgsino-like scenario, gauginolike scenario, and the CMSSM 40.2.2 benchmark point, respectively. As shown in Fig. 8, the cross section of the process $gg \to \tilde{\chi}_1^0 \tilde{g}$ in the CMSSM 40.2.2 benchmark point is about 7.4, 7.1, and 7 times larger than in the gauginolike scenario, Higgsino-like scenario, and mixture-case scenario, respectively. The cross section for $gg \to \tilde{\chi}_2^0 \tilde{g}$ in the CMSSM 40.2.2 benchmark point is about 6.7 times, 2.8 times, and 10% larger than in the gauginolike scenario, mixture-case scenario, and Higgsino-like scenario, respectively.

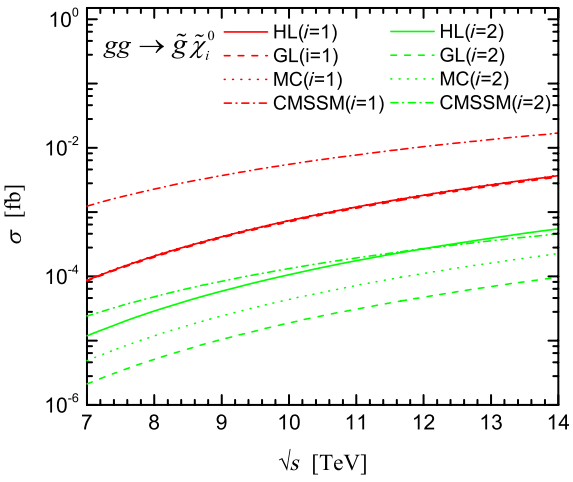

FIG. 8 (color online). Total cross sections of the process $pp(gg) \to \tilde{g} \tilde{\chi}_i^0$ ($i = 1, 2$) versus the center-of-mass energy of pp collider $\sqrt{s}$.

In Table II, the cross sections of single neutralino associated production at center-of-mass energy $\sqrt{s} = 7$ and 14 TeV are given for each scenario. It is clear from this table that the cross section of the process $pp \to \tilde{\chi}_2^0 \tilde{\chi}_1^+$ in the gauginolike scenario yields cross sections of ~600–1700 fb for $\sqrt{s} = 7$ and 14 TeV, which is larger than the remaining ones. Moreover, the cross section for $pp \to \tilde{\chi}_1^0 \tilde{q}_{L,R} (\tilde{\chi}_2^0 \tilde{q}_{L,R})$ reaches about 57(90) fb at $\sqrt{s} =$ 14 TeV in the gauginolike scenario. However, the process $pp(gg) \to \tilde{\chi}_i^0 \tilde{g}$ is suppressed by the others. The magnitudes of the cross sections are at a visible level of 10^0 fb for $pp \to \tilde{\chi}_i^0 \tilde{g}$, 10^1 fb for $pp \to \tilde{\chi}_i^0 \tilde{q}_{L,R}$, 10^{-1}–10^3 fb for $pp \to \tilde{\chi}_i^0 \tilde{\chi}_j^+$, and 10^{-4}–10^{-2} fb for $pp(gg) \to \tilde{\chi}_i^0 \tilde{g}$ at $\sqrt{s} = 14$ TeV. Additionally, it can be easily seen that the cross section for the associated production of the next-to-lightest neutralino $\tilde{\chi}_2^0$ is generally much larger than the cross section for the associated production of the lightest neutralino $\tilde{\chi}_1^0$ for each scenario.

The masses and mixing matrices of the neutralino/chargino depend on the parameters M_2 and μ; therefore, it is so important to study the dependence of the cross section of the single neutralino production on these parameters. Accordingly, we plot the dependence of the total cross section of the associated process in the M_2-μ mass plane with varying M_2 and μ in the range from 100 to 1000 GeV in steps of 50 GeV at center-of-mass energy 8 TeV for

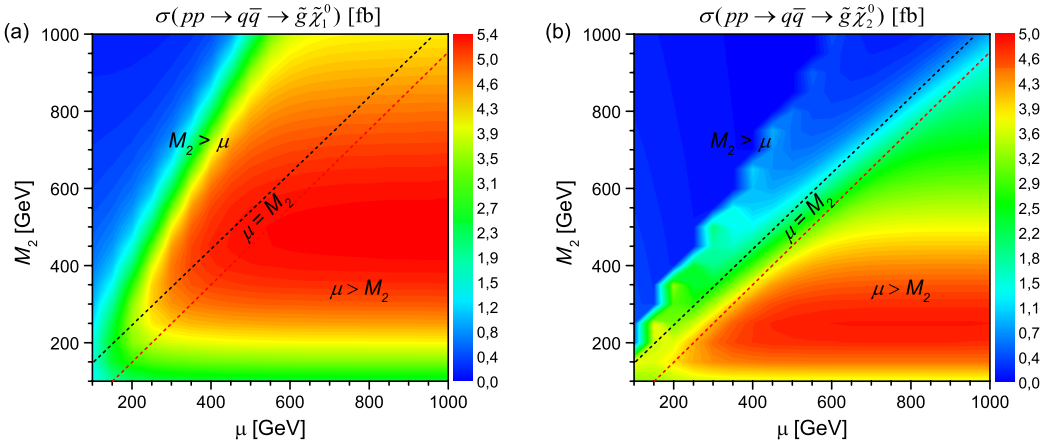

FIG. 9 (color online). Contour plots of the total cross sections of the process (a) $pp \to \tilde{g}\tilde{\chi}_1^0$ and (b) $pp \to \tilde{g}\tilde{\chi}_2^0$ in the $M_2 - \mu$ plane for $\sqrt{s} = 8$ TeV. We choose $\tan\beta = 45$ and fix $M_1 = \frac{5}{3}M_2 \tan^2\theta_W$.

$\tan\beta = 45$, as shown in Figs. 9–12. In these figures, the region above the black dashed line corresponds to $M_2 > \mu$ (Higgsino like), the region below the red dashed line corresponds to $M_2 < \mu$ (gauginolike), and the region between the two dashed lines corresponds to $\mu = M_2$ (mixture case). One can note that these figures reconfirm the dominant scenarios which appear in the dependence of the cross sections on the center-of-mass energy. We can see from Figs. 9 and 10 that the cross sections of the processes $pp \to \tilde{\chi}_i^0\tilde{g}$ and $pp \to \tilde{\chi}_i^0\tilde{q}_{L,R}$ in the M_2-μ mass plane increase during both increasing μ and decreasing M_2. In particular, the maximum values are obtained in the region $200 \lesssim \mu \lesssim 1000$ GeV and $M_2 \lesssim 400$ GeV into the scan region. This case corresponds to the gauginolike scenario. As a result, one can note that the cross section of these processes can be measured experimentally in some scenarios for a lower value of M_2. However, as illustrated in Fig. 11, the cross sections for $pp \to \tilde{\chi}_i^0\tilde{\chi}_j^+$ in the M_2-μ mass plane increase during both decreasing μ and M_2. Here, the maximum values are obtained in the region $\mu \lesssim 400$ GeV and any value of M_2 for processes $pp \to \tilde{\chi}_1^0\tilde{\chi}_1^+$ $(M_2 > \mu)$ and $\tilde{\chi}_2^0\tilde{\chi}_1^+$ $(\mu > M_2)$, while in the regions $100 \lesssim M_2 \lesssim 400$ GeV and $100 \lesssim \mu \lesssim 400$ GeV for processes $pp \to \tilde{\chi}_1^0\tilde{\chi}_2^+$ $(\mu > M_2)$ and $\tilde{\chi}_2^0\tilde{\chi}_2^+$ $(\mu = M_2)$. Note that, as mentioned before, the process of contributions to cross section from not only neutralino mixing matrix, but also chargino mixing matrixes. One can see from Fig. 12 that the dependence of the cross section of the process $gg \to \tilde{\chi}_i^0\tilde{g}$ in the M_2-μ mass plane increases with increasing M_2 and any value of μ. In particular, the cross section of process $gg \to \tilde{\chi}_i^0\tilde{g}$ indicates the maximum values in the region $600 \lesssim M_2 \lesssim 1000$ GeV and $\mu \lesssim 600$ GeV as illustrated in Figs. 12(a) and 12(b). This case corresponds to the Higgsino-like scenario $(M_2 > \mu)$.

In Figs. 13–16 we present the cross section as a function of squark mass for single neutralino production at $\sqrt{s} = 8$ TeV. The total cross section for the single neutralino production processes apart from $pp \to \tilde{\chi}_i^0\tilde{\chi}_j^+$ are essentially determined by the squark masses so that it decreases with increasing the squark mass between 500 and 2000 GeV

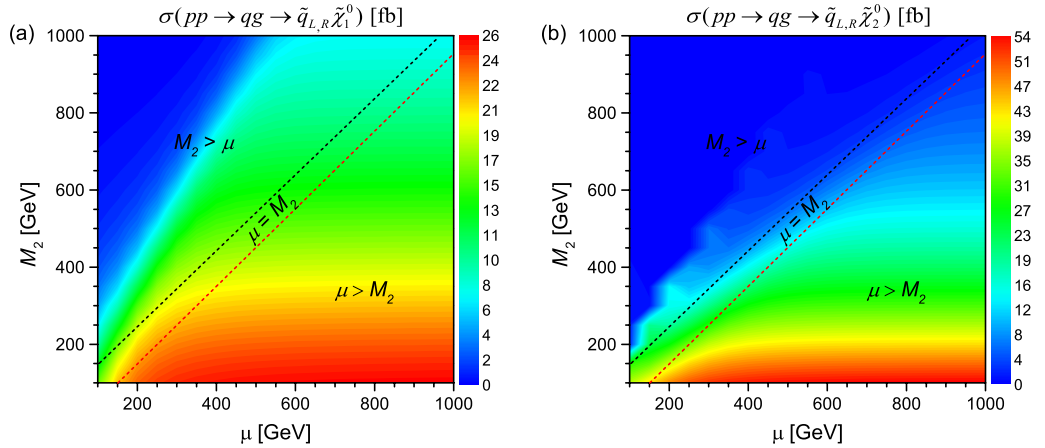

FIG. 10 (color online). Contour plots of the total cross sections of the process (a) $pp \to \tilde{q}_{L,R}\tilde{\chi}_1^0$ and (b) $pp \to \tilde{q}_{L,R}\tilde{\chi}_2^0$ in the $M_2 - \mu$ plane for $\sqrt{s} = 8$ TeV. We choose $\tan\beta = 45$ and fix $M_1 = \frac{5}{3}M_2 \tan^2\theta_W$.

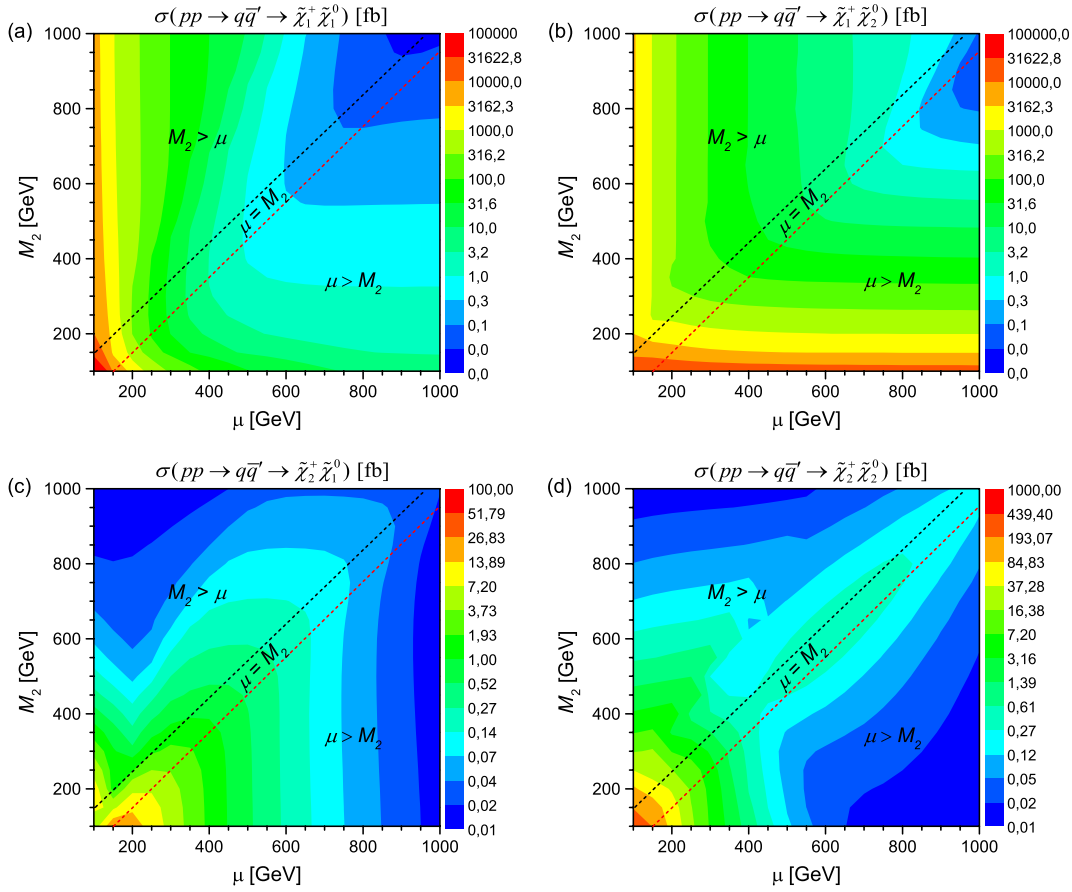

FIG. 11 (color online). Contour plots of the total cross sections of the process (a) $pp \to \tilde{\chi}_1^0 \tilde{\chi}_1^+$, (b) $pp \to \tilde{\chi}_1^0 \tilde{\chi}_2^+$, (c) $pp \to \tilde{\chi}_2^0 \tilde{\chi}_1^+$, and (d) $pp \to \tilde{\chi}_2^0 \tilde{\chi}_2^+$ in the $M_2 - \mu$ plane for $\sqrt{s} = 8$ TeV. We choose $\tan\beta = 45$ and fix $M_1 = \frac{5}{3} M_2 \tan^2\theta_W$.

for each scenario. When the squark mass increases by a factor of 4, the cross section is pulled down by about 1, 3, and 2 orders of magnitude for the processes $pp \to \tilde{\chi}_i^0 \tilde{g}$, $pp \to \tilde{\chi}_i^0 \tilde{q}_{L,R}$, and $pp(gg) \to \tilde{\chi}_i^0 \tilde{g}$, respectively. On the other hand, for the process $pp \to \tilde{\chi}_i^0 \tilde{\chi}_j^+$, the cross section is less affected with respect to variation in the squark mass because the s channel of this process is dominant and together the t- and u-channel terms are suppressed for large squark masses. The cross sections of the single neutralino production for the squark mass 1 and 2 TeV at $\sqrt{s} = 8$ TeV

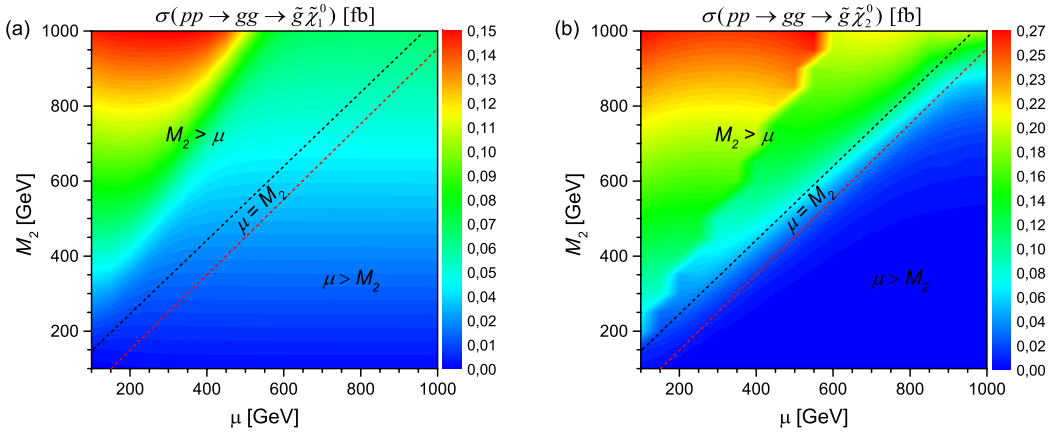

FIG. 12 (color online). Contour plots of the total cross sections of the process (a) $pp(gg) \to \tilde{g}\tilde{\chi}_1^0$ and (b) $pp(gg) \to \tilde{g}\tilde{\chi}_2^0$ in the $M_2 - \mu$ plane for $\sqrt{s} = 8$ TeV. We choose $\tan\beta = 45$ and fix $M_1 = \frac{5}{3} M_2 \tan^2\theta_W$.

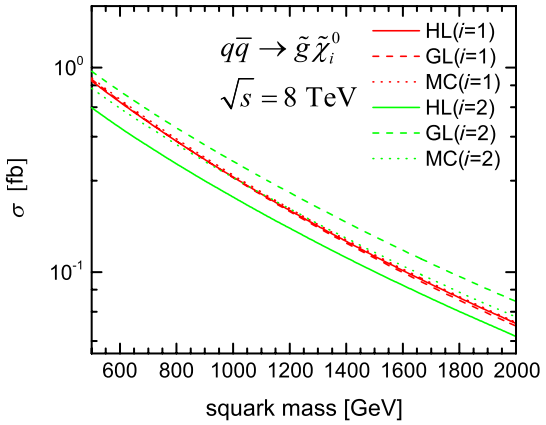

FIG. 13 (color online). Total cross sections for the process $pp \to \tilde{g}\tilde{\chi}_i^0$ $(i = 1, 2)$ depending on the squark mass at $\sqrt{s} = 8$ TeV.

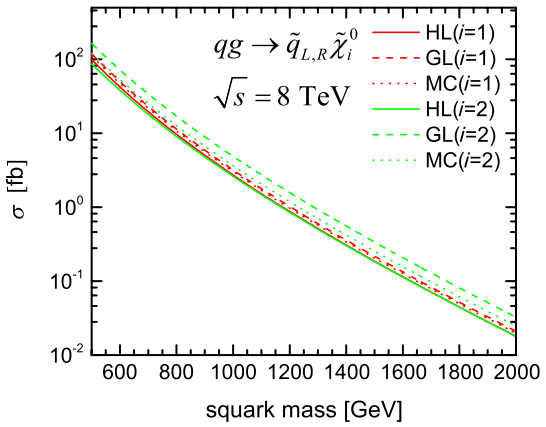

FIG. 14 (color online). Total cross sections of the process $pp \to \tilde{q}_{L,R}\tilde{\chi}_i^0$ $(i = 1, 2)$ depending on the squark mass at $\sqrt{s} = 8$ TeV.

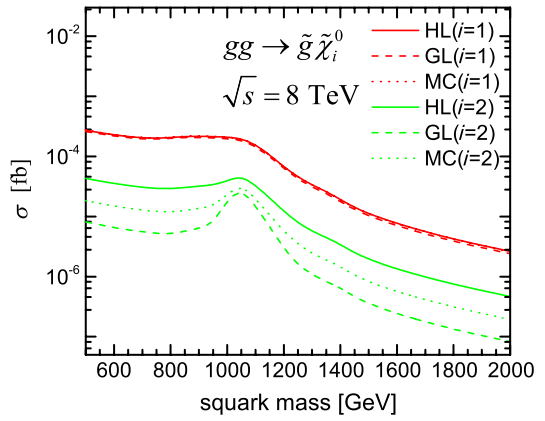

FIG. 16 (color online). Total cross sections of the process $pp(\mathrm{gg}) \to \tilde{g}\tilde{\chi}_i^0$ $(i = 1, 2)$ depending on the squark mass at $\sqrt{s} = 8$ TeV.

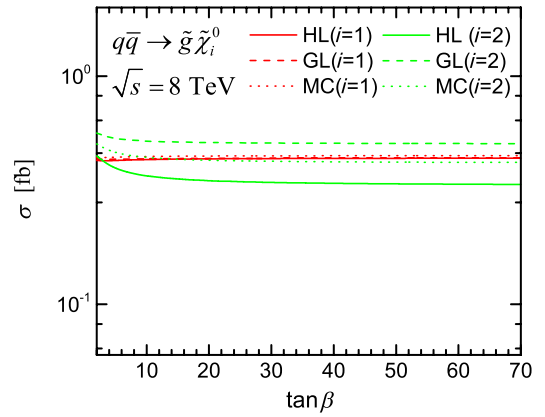

FIG. 17 (color online). Total cross sections of the process $pp \to \tilde{g}\tilde{\chi}_i^0$ $(i = 1, 2)$ as a function of $\tan\beta$ at $\sqrt{s} = 8$ TeV.

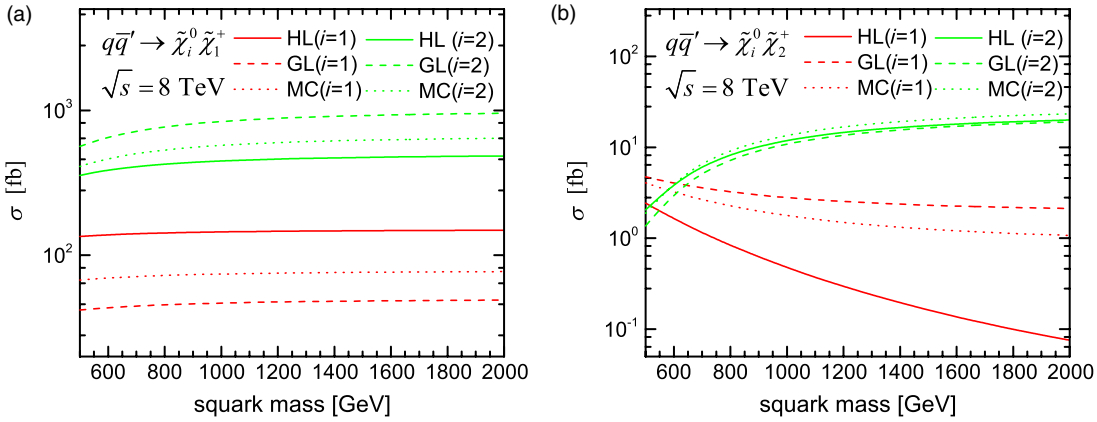

FIG. 15 (color online). Total cross sections of the processes $pp \to \tilde{\chi}_i^0\tilde{\chi}_1^+$ (left) and $\tilde{\chi}_i^0\tilde{\chi}_2^+$ (right) $(i = 1, 2)$ depending on the squark mass at $\sqrt{s} = 8$ TeV.

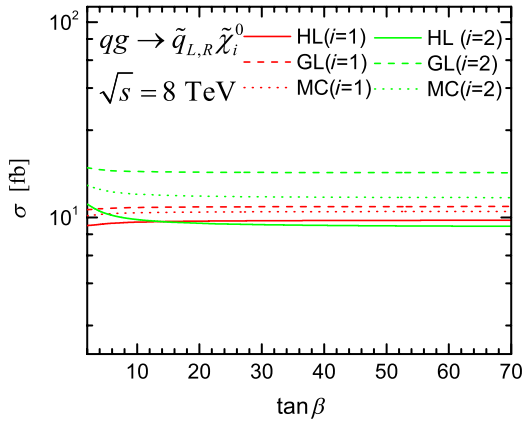

FIG. 18 (color online). Total cross sections of the process $pp \to \tilde{q}_{L,R}\tilde{\chi}_i^0$ ($i = 1, 2$) as a function of $\tan\beta$ at $\sqrt{s} = 8$ TeV.

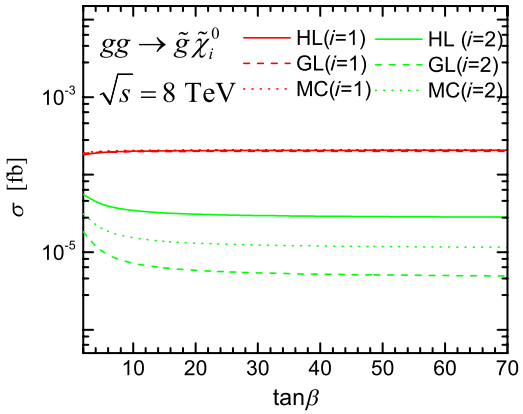

FIG. 20 (color online). Total cross sections of the process $pp(\mathrm{gg}) \to \tilde{\mathrm{g}}\tilde{\chi}_i^0$ ($i = 1, 2$) as a function of $\tan\beta$ at $\sqrt{s} = 8$ TeV.

so as to facilitate precise comparisons with the experimental results are summarized in Table III. As seen from this table, the dependence of cross section on the squark mass is dominated by one of the processes, $pp \to \tilde{\chi}_2^0\tilde{\chi}_1^+$ appears 0.95 pb for the squark mass 2 TeV in the gauginolike scenario.

Finally, the $\tan\beta$ dependence of the cross sections for the single neutralino processes are depicted in Figs. 17–20. From these figures we can clearly see that cross sections of the processes $pp \to \tilde{\chi}_i^0\tilde{\mathrm{g}}$, $pp \to \tilde{\chi}_i^0\tilde{q}_{L,R}$, and $\mathrm{gg} \to \tilde{\chi}_i^0\tilde{\mathrm{g}}$ increase (decrease) slowly for $i = 1$ ($i = 2$) when $\tan\beta$ goes up from 2 to 10, and vary smoothly when $\tan\beta > 10$ for each scenario. However, the cross sections of the processes $pp \to \tilde{\chi}_i^0\tilde{\chi}_j^+$ apart from $pp \to \tilde{\chi}_1^0\tilde{\chi}_2^+$ decrease with increasing the $\tan\beta$ from 2 to 70. Moreover, there appear the same dominant scenarios as in the dependence of the cross sections on the center-of-mass energy.

The possible contributions to the background in the signal regions come from the Standard Model processes as $pp \to WW$, $pp \to ZZ$, $pp \to WZ$, and $pp \to t\bar{t}$. If we are interested in signals with leptons in the final state, then in the case of $1l + \not{E}_T +$ jets mode, the background appears from $pp \to WW$, $pp \to WZ$, and $pp \to t\bar{t}$, Also, the processes $pp \to ZZ$, $pp \to WW$, and $pp \to t\bar{t}$ can yield background for the $2l + \not{E}_T +$ jets mode. The process $pp \to WZ$ can yield background for the $3l + \not{E}_T +$ 0 jets decay mode. Of course, all background channels could have large cross sections, but despite this it needs some additional cutoff mechanism that will help for the extraction, as mentioned above. An analysis of our calculations is shown since those background channels can have large cross sections. It should be noted that, in our case, the background cross section is about 1–3 orders of magnitude larger than the signal. We hope the at $\sqrt{s} = 14$ TeV with integrated luminosity $L_{\mathrm{int}} = 100$ fb^{-1}, the total cross section of single neutralino production in the gauginolike case could be observable at the LHC. It should be noted that some problems within the E_6 model are discussed in Ref. [39].

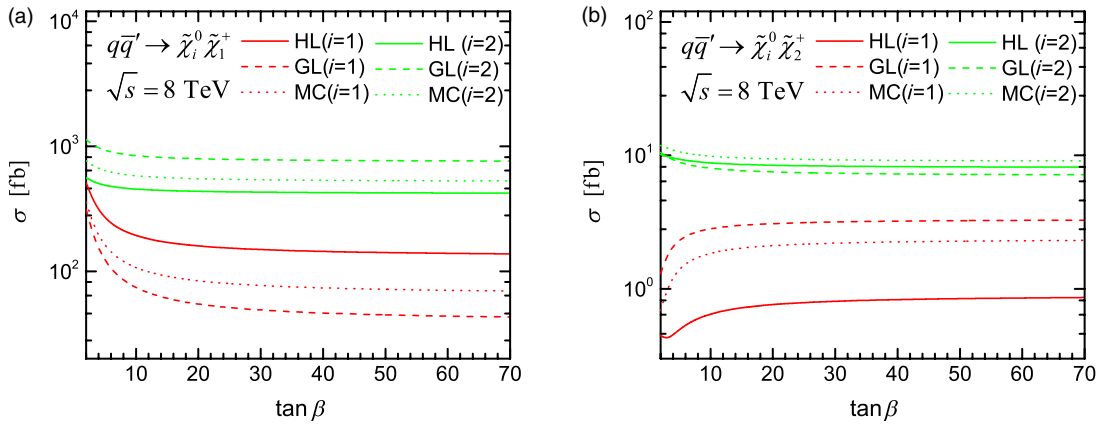

FIG. 19 (color online). Total cross sections of the processes $pp \to \tilde{\chi}_i^0\tilde{\chi}_1^+$ (left) and $\tilde{\chi}_i^0\tilde{\chi}_2^+$ (right) ($i = 1, 2$) as a function of $\tan\beta$ at $\sqrt{s} = 8$ TeV.

TABLE II. Total cross sections (in fb) for the single neutralino production at center-of-mass energy $\sqrt{s} = 7$ and 14 TeV.

	Higgsino like		Gaugino like		Mixture case		CMSSM 40.2.2	
σ (process) (fb)	7 TeV	14 TeV	7 TeV	14 TeV	7 TeV	14 TeV	7 TeV	14 TeV
$\sigma(pp \to \tilde{\chi}_1^0 \tilde{g})$	0.22	3.70	0.22	3.61	0.23	3.75	3.66	22.44
$\sigma(pp \to \tilde{\chi}_2^0 \tilde{g})$	0.17	3.13	0.25	4.80	0.21	3.97	3.15	24.79
$\sigma(pp \to \tilde{\chi}_1^0 \tilde{q}_{L,R})$	6.07	48.66	7.18	56.59	6.75	53.67	1.11	16.07
$\sigma(pp \to \tilde{\chi}_2^0 \tilde{q}_{L,R})$	5.63	47.82	10.50	89.95	7.84	67.33	1.22	23.31
$\sigma(pp \to \tilde{\chi}_1^0 \tilde{\chi}_1^+)$	117.92	296.75	37.83	93.53	60.10	150.75	0.24	0.80
$\sigma(pp \to \tilde{\chi}_2^0 \tilde{\chi}_1^+)$	346.94	922.03	629.53	1654.78	434.16	1157.26	59.10	163.32
$\sigma(pp \to \tilde{\chi}_1^0 \tilde{\chi}_2^+)$	0.64	2.24	2.56	7.67	1.78	5.52	0.06	0.22
$\sigma(pp \to \tilde{\chi}_2^0 \tilde{\chi}_2^+)$	6.54	19.11	5.78	16.64	7.31	21.11	0.01	0.04
$\sigma(pp \to \tilde{\chi}_1^0 \tilde{g})_{\text{one loop}}$	$\mathcal{O}(10^{-4})$	$\mathcal{O}(10^{-3})$	$\mathcal{O}(10^{-4})$	$\mathcal{O}(10^{-3})$	$\mathcal{O}(10^{-4})$	$\mathcal{O}(10^{-3})$	$\mathcal{O}(10^{-3})$	0.02
$\sigma(pp \to \tilde{\chi}_2^0 \tilde{g})_{\text{one loop}}$	$\mathcal{O}(10^{-5})$	$\mathcal{O}(10^{-4})$	$\mathcal{O}(10^{-6})$	$\mathcal{O}(10^{-4})$	$\mathcal{O}(10^{-6})$	$\mathcal{O}(10^{-4})$	$\mathcal{O}(10^{-5})$	$\mathcal{O}(10^{-4})$

TABLE III. Total cross sections (in fb) for the single neutralino production processes as a function of the squark mass at $\sqrt{s} = 8$ TeV.

	$m_{\tilde{q}}$ (GeV)	$\tilde{\chi}_1^0 \tilde{g}$	$\tilde{\chi}_2^0 \tilde{g}$	$\tilde{\chi}_1^0 \tilde{q}$	$\tilde{\chi}_2^0 \tilde{q}$	$\tilde{\chi}_1^0 \tilde{\chi}_1^+$	$\tilde{\chi}_2^0 \tilde{\chi}_1^+$	$\tilde{\chi}_1^0 \tilde{\chi}_2^+$	$\tilde{\chi}_2^0 \tilde{\chi}_2^+$	$\tilde{\chi}_1^0 \tilde{g}_{\text{one loop}}$	$\tilde{\chi}_2^0 \tilde{g}_{\text{one loop}}$
HL	1000	0.29	0.23	2.72	2.62	144.90	447.40	0.48	11.85	2.07×10^{-5}	4.16×10^{-6}
	2000	0.06	0.05	0.02	0.02	148.73	484.43	0.08	19.92	2.61×10^{-7}	4.93×10^{-8}
GL	1000	0.29	0.35	3.19	4.87	46.78	838.21	2.79	10.86	1.95×10^{-5}	1.96×10^{-6}
	2000	0.05	0.07	0.02	0.03	49.01	954.97	2.13	18.99	2.36×10^{-7}	0.86×10^{-8}
MC	1000	0.30	0.29	3.01	3.65	74.26	573.41	1.77	13.53	2.08×10^{-5}	2.45×10^{-6}
	2000	0.06	0.06	0.02	0.03	77.10	642.44	1.07	23.31	2.57×10^{-7}	2.02×10^{-8}

IV. CONCLUSION

In the present paper, we have concentrated on the single neutralino production processes $pp \to \tilde{\chi}_i^0 \tilde{g}$, $pp \to \tilde{\chi}_i^0 \tilde{q}_{L,R}$, $pp \to \tilde{\chi}_i^0 \tilde{\chi}_j^+$ at tree level and one loop $pp(gg) \to \tilde{\chi}_i^0 \tilde{g}$ at the LHC. Cross sections of these processes have been calculated by the CMSSM 40.2.2 benchmark point and three different scenarios named the Higgsino-like, gauginolike, and mixture cases. From our calculations, we have obtained that in these cases, the gauginolike scenario was more dominant relative to the other scenarios. Additionally, the processes $pp \to \tilde{\chi}_1^0 \tilde{\chi}_1^+$ and $\tilde{\chi}_2^0 \tilde{\chi}_1^+$ dominated over the other single neutralino production processes by roughly 2–3 orders of magnitude. In particular, the cross section of the process $pp \to \tilde{\chi}_2^0 \tilde{\chi}_1^+$ in the gauginolike scenario ($\tilde{\chi}_1^0 \tilde{\chi}_1^+$ in the Higgsino-like scenario) appeared in the range of $\sim$0.63(0.12) pb to $\sim$1.65(0.30) pb with increasing center-of-mass energy from 7 to 14 TeV. One may argue that the investigation of these two processes for the single neutralino production at proton-proton collisions is significant in both experimental and theoretical research. According to our opinion, these may be used as a probe for an experimental search on the single neutralino production in the LHC and also in the future colliders. It is clear that the results discussed in the parameter scan depend strongly on the assumptions taken into consideration, like the M_2 and μ parameters. The CMSSM scenario has different character, which is more like the Higgsino-like and mixture cases. In general, our scenarios dominate over the CMSSM 40.2.2 benchmark scenario. Thus, taking into account the predictions of our study in the LHC, single neutralino production processes are more likely to be observed. Observables should then be constructed addressing gluino, squark, and neutralino decay channels to various numbers of leptons and jets; as such, the $\tilde{q} \to q \tilde{\chi}_1^0$ and $\tilde{g} \to q \bar{q} \tilde{\chi}_1^0$ cascade decays to weakly interacting neutralino which escape the detector unseen. Also, we hope our results will help explain the expectation results in the LHC and future linear collider.

ACKNOWLEDGMENTS

A. I. A. is grateful for the financial support of TUBITAK Grant No. 2221 (Turkey) and Baku State University Grant No. "50+50." The authors acknowledge the interest of the members of the Department of Physics of Karadeniz Technical University.

APPENDIX: THE NEUTRALINO/CHARGINO SECTOR OF THE MSSM

The neutralino mass eigenstates $\tilde{\chi}_i^0$ ($i = 1, \ldots, 4$) are the linear superposition of the gauginos $\tilde{B}$, $\tilde{W}^3$, and the

Higgsinos $\tilde{H}_1^0$, $\tilde{H}_2^0$ in the MSSM. The neutralinos mass term in the MSSM Lagrangian is expressed as [3]

$$\mathcal{L} = -\frac{1}{2}(\psi_i^0)^T \mathcal{M} \psi_j^0 + \text{H.c.}, \tag{A1}$$

which is bilinear in the fermion fields $\psi_j^0 = (-i\tilde{B}, -i\tilde{W}^3, \tilde{H}_1^0, \tilde{H}_2^0)^T$ with $j = 1, \ldots, 4$. The neutralino mass matrix, which is generally a complex and symmetric matrix, is explicitly given by

$$\mathcal{M} = \begin{pmatrix} M_1 & 0 & -m_Z c_\beta s_W & m_Z s_\beta s_W \\ 0 & M_2 & m_Z c_\beta c_W & -m_Z s_\beta c_W \\ -m_Z c_\beta s_W & m_Z c_\beta c_W & 0 & -\mu \\ m_Z s_\beta s_W & -m_Z s_\beta c_W & -\mu & 0 \end{pmatrix}, \tag{A2}$$

where M_1 and M_2 are the gaugino mass parameters corresponding to the $U(1)$ and $SU(2)$ subgroups, separately, μ is the Higgsino mass parameter, and $\tan\beta = v_2/v_1$ is equal to the ratio of the vacuum expectation values $v_{1,2}$ of the two Higgs doublets, which break the electroweak symmetry. These mass parameters are complex in CP-noninvariant theories. The mass parameter M_2 could be achieved by the reparametrization of the fields as real and positive without any loss of generality so that the two remaining nontrivial phases, which are reparametrization invariant, could be associated with M_1 and μ as follows: $M_1 = |M_1|e^{i\phi_1}$ and $\mu = |\mu|e^{i\phi_\mu}$, $(0 \leq \phi_1, \phi_\mu < 2\pi)$.

The neutralino mass matrix $\mathcal{M}$ is diagonalized by a 4×4 unitary matrix N, which is adequate to transform from the gauge eigenstate basis $(\tilde{B}, \tilde{W}^3, \tilde{H}_1^0, \tilde{H}_2^0)$ to the mass eigenstate basis of the Majorana fields $\tilde{\chi}_i^0$ such that,

$$\mathcal{M}_D = N^T \mathcal{M} N = \sum_{j=1}^{4} m_{\tilde{\chi}_j^0} E_j. \tag{A3}$$

The relation between the weak and physical neutralinos' eigenstates is expressed by $\chi_i^0 = N_{ij}\psi_j^0$. For determining of the mixing matrix N, we get the square of the Eq. (A3) as follows:

$$\mathcal{M}_D^2 = N^{-1}\mathcal{M}^+\mathcal{M}N = \sum_{j=1}^{4} m_{\tilde{\chi}_j^0}^2 E_j, \tag{A4}$$

where $(E_j)_{ik} = \delta_{ji}\delta_{jk}$. The neutralino mass eigenvalues $m_{\tilde{\chi}_j^0}$ in $\mathcal{M}_D$ could be gotten as real and positive by an appropriate definition of the unitary matrix N. From Eq. (A4), we get

$$(\mathcal{M}^+\mathcal{M})N - N\mathcal{M}_D^2 = 0, \tag{A5}$$

and then considering the following relation

$$|N_{1j}|^2 + |N_{2j}|^2 + |N_{3j}|^2 + |N_{4j}|^2 = 1, \tag{A6}$$

the unitary matrix N_{ij} is determined from the system of equations in Eq. (A5) (see Ref. [40] for details). Moreover, the neutralino masses are solutions of the characteristic equation related to this system, which is

$$X^4 - aX^3 + bX^2 - cX + d = 0. \tag{A7}$$

After solution Eq. (A7), one is able to get the exact analytical expressions for the neutralino masses as follows:

$$\begin{aligned} m_{\tilde{\chi}_1^0}^2, m_{\tilde{\chi}_2^0}^2 &= \frac{a}{4} - \frac{f}{2} \mp \frac{1}{2}\sqrt{r - w - \frac{p}{4f}}, \\ m_{\tilde{\chi}_3^0}^2, m_{\tilde{\chi}_4^0}^2 &= \frac{a}{4} + \frac{f}{2} \mp \frac{1}{2}\sqrt{r - w + \frac{p}{4f}}, \end{aligned} \tag{A8}$$

where

$$\begin{aligned} f &= \sqrt{\frac{r}{2} + w}, \qquad r = \frac{a^2}{2} - \frac{4b}{3}, \\ w &= \frac{q}{(3 \cdot 2^{1/3})} + \frac{(2^{1/3} \cdot h)}{3 \cdot q}, \qquad p = a^3 - 4ab + 8c, \\ q &= \left(k + \sqrt{k^2 - 4h^3}\right)^{1/3}, \\ k &= 2b^3 - 9abc + 27c^2 + 27a^2 d - 72bd, \\ h &= b^2 - 3ac + 12d. \end{aligned} \tag{A9}$$

The chargino mass eigenstates $\tilde{\chi}_j^\pm$ $(j = 1, 2)$ are the linear superposition of the gauginos $\tilde{W}^\pm$ and the Higgsinos $H_{2,1}^\pm$. In terms of two-component Weyl spinors, the chargino mass term in the Lagrangian can be written as [3]

$$\mathcal{L} = -\frac{1}{2}(\psi^+ \quad \psi^-)\begin{pmatrix} 0 & \mathcal{M}_C^T \\ \mathcal{M}_C & 0 \end{pmatrix}\begin{pmatrix} \psi^+ \\ \psi^- \end{pmatrix} + \text{H.c.}, \tag{A10}$$

which is bilinear in the fermionic fields $\psi_j^\pm = (-i\tilde{W}^\pm, \tilde{H}_{2,1}^\pm)^T$. The chargino mass matrix $\mathcal{M}_C$ is given by

$$\mathcal{M}_C = \begin{pmatrix} M_2 & \sqrt{2}m_W c_\beta \\ \sqrt{2}m_W s_\beta & |\mu|e^{i\phi_\mu} \end{pmatrix}. \tag{A11}$$

As seen from Eq. (A11), the matrix $\mathcal{M}_C$ is not symmetric; it can be diagonalized analytically by two different unitary matrices V and U such that these satisfy the relation $U^*\mathcal{M}_C V^{-1} = \text{diag}\{m_{\tilde{\chi}_1^\pm}, m_{\tilde{\chi}_2^\pm}\}$ with the chargino mass eigenvalues as follows:

$$\begin{aligned} m_{\tilde{\chi}_{1,2}^+}^2 = \frac{1}{2}\{&M_2^2 + |\mu|^2 + 2m_W^2 \mp [(M_2^2 - |\mu|^2 - 2m_W^2\cos 2\beta)^2 \\ &+ 8m_W^2(M_2^2 c_\beta^2 + |\mu|^2 s_\beta^2 + M_2|\mu|\sin 2\beta\cos\phi_\mu)]^{1/2}\}. \end{aligned} \tag{A12}$$

In this paper, we take into consideration the gaugino/Higgsino sector with the following assumptions: We set $\phi_1 = \phi_\mu = 0$ for CP conservation. The physical signs between μ, M_1, and M_2 are relative, which could be absorbed into phases ϕ_1 and ϕ_μ by rearranging of fields. Therefore, μ, M_1, and M_2 are chosen to be real and positive, which are usually assumed to be related via the relation $M_1 = \frac{5}{3} M_2 \tan^2\theta_W \simeq 0.5 M_2$. Using these assumptions, there appear several scenarios for the choice of the SUSY parameters. On account of the fact that SUSY parameters should be obtained from physical quantities, it is also possible that we choose an alternative way to diagonalize the mass matrix $\mathcal{M}$ by taking any two chargino masses together with $\tan\beta$ as inputs. In this case, the two mass parameters M_2 and μ can be calculated from the chargino masses for given $\tan\beta$ [41,42]. By taking the appropriate sums and differences of the chargino masses, one can obtain the following solutions for M_2 and μ:

$$M_2^2 = \frac{1}{2}\Big((m_{\tilde{\chi}_1^+}^2 + m_{\tilde{\chi}_2^+}^2 - 2m_W^2) \mp \sqrt{(m_{\tilde{\chi}_1^+}^2 + m_{\tilde{\chi}_2^+}^2 - 2m_W^2)^2 - \Delta_\pm}\Big), \tag{A13}$$

$$|\mu|^2 = \frac{1}{2}\Big((m_{\tilde{\chi}_1^+}^2 + m_{\tilde{\chi}_2^+}^2 - 2m_W^2) \pm \sqrt{(m_{\tilde{\chi}_1^+}^2 + m_{\tilde{\chi}_2^+}^2 - 2m_W^2)^2 - \Delta_\pm}\Big), \tag{A14}$$

with

$$\Delta_\pm = 4\Big[m_{\tilde{\chi}_1^+}^2 m_{\tilde{\chi}_2^+}^2 + m_W^4 \cos 2\phi_\mu \sin^2 2\beta \pm 2m_W^2 \cos\phi_\mu \sin 2\beta \times \sqrt{m_{\tilde{\chi}_1^+}^2 m_{\tilde{\chi}_2^+}^2 - m_W^4 \sin^2 2\beta \sin^2\phi_\mu}\Big],$$

where the lower (upper) signs correspond to the $M_2 > |\mu|$ ($M_2 < |\mu|$) regime. So, for given $\tan\beta$, μ, and M_2, terms of the two chargino masses $m_{\tilde{\chi}_1^+}$ and $m_{\tilde{\chi}_2^+}$ are obtained by using Eqs. (A13) and (A14) from which one can derive four solutions corresponding to different physical scenarios. For $|\mu| < M_2$, the lightest chargino has a stronger Higgsino-like component and so it is named Higgsino-like [42,43]. Furthermore, the solution $|\mu| > M_2$, corresponding to the gauginolike situation could be easily gotten by the replacements as follows: $\mu \to \mathrm{sign}(\mu) M_2$ and $M_2 \to |\mu|$ [43,44].

[1] Y. A. Golfand and E. P. Likhtman, JETP Lett. **13**, 323 (1971); A. Neveu and J. H. Schwartz, Nucl. Phys. **B31**, 86 (1971); Phys. Rev. D **4**, 1109 (1971); P. Ramond, Phys. Rev. D **3**, 2415 (1971); J. Wess and B. Zumino, Nucl. Phys. **B70**, 39 (1974).

[2] H. P. Nilles, Phys. Rep. **110**, 1 (1984).

[3] H. E. Haber and G. L. Kane, Phys. Rep. **117**, 75 (1985).

[4] D. I. Kazakov, Phys. Rep. **344**, 309 (2001).

[5] G. R. Farrar and P. Fayet, Phys. Lett. **76B**, 575 (1978).

[6] S. P. Martin, Phys. Rev. D **46**, R2769 (1992); E. Diehl, G. L. Kane, C. Kolda, and J. D. Wells, Phys. Rev. D **52**, 4223 (1995).

[7] H. Goldberg, Phys. Rev. Lett. **50**, 1419 (1983); J. Ellis, J. S. Hagelin, D. V. Nanopoulos, K. A. Olive, and M. Srednicki, Nucl. Phys. **B238**, 453 (1984).

[8] G. Bertone, D. Hooper, and J. Silk, Phys. Rep. **405**, 279 (2005).

[9] H. Baer, A. Mustafayev, H. Summy, and X. Tata, J. High Energy Phys. 10 (2007) 088, and references therein; B. Herrmann and M. Klasen, Phys. Rev. D **76**, 117704 (2007).

[10] https://twiki.cern.ch/twiki/bin/view/AtlasPublic.

[11] https://twiki.cern.ch/twiki/bin/view/CMSPublic/PhysicsResults.

[12] J. Abdallah *et al.* (DELPHI Collaboration), Eur. Phys. J. C **31**, 421 (2003).

[13] J. Beringer *et al.* (Particle Data Group), Phys. Rev. D **86**, 010001 (2012).

[14] H. Baer, D. D. Karatas, and X. Tata, Phys. Rev. D **42**, 2259 (1990).

[15] E. L. Berger, M. Klasen, and T. M. P. Tait, Phys. Rev. D **62**, 095014 (2000).

[16] B. C. Allanach, S. Grab, and H. E. Haber, J. High Energy Phys. 01 (2011) 138; 07 (2011) 087(E); 09 (2011) 027(E).

[17] T. Binoth, D. G. Netto, D. Lopes-Val, K. Mawatari, T. Plehn, and I. Wigmore, Phys. Rev. D **84**, 075005 (2011).

[18] W. Beenakker, M. Klasen, M. Krämer, T. Plehn, M. Spira, and P. M. Zerwas, Phys. Rev. Lett. **83**, 3780 (1999).

[19] J. Debove, B. Fuks, and M. Klasen, Phys. Rev. D **78**, 074020 (2008).

[20] G. J. Gounaris, J. Layssac, P. I. Porfyriadis, and F. M. Renard, Phys. Rev. D **71**, 075012 (2005).

[21] J. F. Gunion and H. E. Haber, Nucl. Phys. **B272**, 1 (1986); **B402**, 567(E) (1993).

[22] J. Rosiek, Phys. Rev. D **41**, 3464 (1990); arXiv:hep-ph/9511250.

[23] W. Greiner, S. Schramm, and E. Stein, *Quantum Chromodynamics* (Springer, Berlin, 2007), 3rd ed.

[24] J. Küblbeck, M. Böhm, and A. Denner, Comput. Phys. Commun. **60**, 165 (1990); J. Küblbeck, H. Eck, and R. Merting, Nucl. Phys. Proc. Suppl. **29A**, 204 (1992); T. Hahn, Comput. Phys. Commun. **140**, 418 (2001).

[25] T. Hahn and C. Schappacher, Comput. Phys. Commun. **143**, 54 (2002).

[26] T. Hahn, Comput. Phys. Commun. **178**, 217 (2008); S. Agrawal, T. Hahn, and E. Mirabella, Proc. Sci., LL2012 (2012) 046.

[27] T. Hahn and M. Perez-Victoria, Comput. Phys. Commun. **118**, 153 (1999).
[28] F. del Aguila, A. Culatti, R. Munoz Tapia, and M. Perez-Victoria, Nucl. Phys. **B537**, 561 (1999).
[29] W. Siegel, Phys. Lett. **84B**, 193 (1979).
[30] D. Capper, D. Jones, and P. van Nieuwenhuizen, Nucl. Phys. **B167**, 479 (1980).
[31] D. Stöckinger, J. High Energy Phys. 03 (2005) 076.
[32] S. S. AbdusSalam, B. C. Allanach *et al.*, Eur. Phys. J. C **71**, 1835 (2011).
[33] A. H. Chamseddine, R. L. Arnowitt, and P. Nath, Phys. Rev. Lett. **49**, 970 (1982).
[34] R. L. Arnowitt and P. Nath, Phys. Rev. Lett. **69**, 725 (1992).
[35] G. L. Kane, C. Kolda, L. Roszkowski, and J. D. Wells, Phys. Rev. D **49**, 6173 (1994).
[36] M. Drees and S. P. Martin, Report No. MADPH-95-879.
[37] B. C. Allanach, Comput. Phys. Commun. **143**, 305 (2002).
[38] A. D. Martin, W. J. Stirling, R. S. Thorne, and G. Watt, Eur. Phys. J. C **63**, 189 (2009).
[39] M. Frank, L. Selbuz, and I. Turan, arXiv:1212.4428.
[40] A. I. Ahmadov, I. Boztosun, R. Kh. Muradov, A. Soylu, and E. A. Dadashov, Int. J. Mod. Phys. E **15**, 1183 (2006).
[41] S. Y. Choi, A. Djouadi, M. Guchait, J. Kalinowski, H. S. Song, and P. M. Zerwas, Eur. Phys. J. C **14**, 535 (2000).
[42] G. Moultaka, in *Proceedings of the 29th International Conference on High-Energy Physics (ICHEP 98), Vancouver, Canada, 1998* [Vancouver High Energy Phys. 2, 1703 (1998)].
[43] S. Y. Choi, J. Kalinowski, G. Moortgat-Pick, and P. M. Zerwas, Eur. Phys. J. C **22**, 563 (2001); **23**, 769(E) (2002).
[44] J. L. Kneur and G. Moultaka, Phys. Rev. D **59**, 015005 (1998).